Addis Ababa University
Addis Ababa Institute of Technology
School of Mechanical and Industrial Engineering

Numerical Modeling of the Residual Stress Induced by multi-impact Shot Peening process on Carburized Fe-0.85Mo-0.35C and Fe-1.5Mo-0.3C Steel Materials

A thesis is submitted to the School of Graduate Studies of Addis Ababa University in partial fulfillment of the Requirement for the Masters of Science in Mechanical Design Engineering

Prepared By:

Esmael Endris Zeleke

Advisor:

Dr. Samuel Tesfaye

2023 G.c

Addis Ababa, Ethiopia

Deceleration

I declare that the thesis entitled "**Numerical Modeling of the Residual Stress Induced by multi-impact Shot Peening process on Carburized Fe-0.85Mo-0.35C and Fe-1.5Mo-0.3C Steel Materials**" has been composed by myself and all the resource of materials used for this thesis have been duly acknowledged. The thesis has not been submitted in any previous application for a degree at any higher educational institution.

Esmael Endris Zeleke	_____	_____
Name of candidate	Signature	Date

This is to certify that the above declaration made by the candidate is correct to the best of my knowledge.

Samuel Tesfaye (Ph.D.)	_____	_____
Advisor	Signature	Date

Addis Ababa University

Addis Ababa institute of Technology

School of Mechanical and Industrial Engineering

Numerical Modeling of the Residual Stress Induced by multi-impact Shot Peening process on Carburized Fe-0.85Mo-0.35C and Fe-1.5Mo-0.3C Steel Materials

By: Esmael Endris Zeleke

Approved by Board of Examiners:

Samuel Tesfaye (Ph.D.)	_____	_____
Advisor	Signature	Date
Haileleoul Sahle (Ph. D)	_____	_____
Internal Examiner	Signature	Date
Getasew Ashagrie (Ph. D)	_____	_____
External Examiner	Signature	Date
Araya Abera (Ph. D)	_____	_____
SMIE Dean	Signature	Date
Sosina Mengistu (Ph. D)	_____	_____
Postgraduate Director	Signature	Date

Acknowledgement

First and foremost, I would like to praise and thank God, the almighty, for giving me countless blessing, knowledge, strength, and opportunity to achieve my goal and accomplish the thesis.

Then I would like to express my deep gratitude to my advisor, Dr. Samuel Tesfaye, assistant professor in Addis Ababa institute technology for his continuous support.

Finally, I would like to express my gratitude to all those who support me in accomplishing this thesis.

Abstract

Shot peening is a surface treatment process in which a large number of small shots are impact an engineering component to generate a compressive residual stress layer at the surface of the component. The compressive residual stress increase fatigue life, resistance to stress corrosion, refine grain size, improve microhardness and prevent crack propagation on the component. However, improper shot peening process parameters would affect the surface quality, and have negative effect on the fatigue performance. The experimental assessment of shot peening process parameters is not only very complex but costly as well. In this paper, a sequential model of multiple-shot impacts has been established to investigate the shot peening process on a carburized prealloyed Fe-0.85Mo-0.35C and Fe-1.5Mo-0.3C steels. A commercial Finite Element Method ABAQUS/Explicit was used to model and simulate the process. The sequential model was applied for the predication of residual stress along the depth profile was obtained in the impact region. Furthermore, the numerical results of compressive residual stress were compared with the experimental result obtained using the x-ray diffraction (XRD) analysis. A parametric study is conducted to investigate the effect of shot velocity, diameter, initial stress and coverage on the residual stress profile. The result demonstrated that increasing shot velocity, diameter and coverage results an increase the surface compressive residual stress and decrease depth of compressive residual layer. On the other hand, initial residual stress increase depth of compressive residual stress layer. The simulation result was in good agreement with the measured result for both steels.

Keywords: Shot peening, Residual stress field, Parametric study, Numerical Simulations.

Table of Contents

List of Figures

List of tables

Nomenclatures

$C_{(t)}$	Coverage
$\dot{m}$	Mass Flow Rate
t	Peening Time
A	Shot Peened Area
r	Radius of Shot
ρ_s and ρ_t	Density of shot and target
c	Lattice Spacing
S	X-Ray Source
D	X-Ray Detector
2θ	Diffraction Angle
N	Angle between incident and diffracted beam bisector, and the normal of the surface
Ψ	Orientation of sample angle
σ_{sur}^{r} and σ_{max}^{r}	surface and maximum residual stress
d_b and d_T	Maximum and total Compressive Residual Stress Depth
HV_s and HV_m	Hardness of Shots and target, respectively
d	Shot Diameter
F_t	Force Acting Any Instant
V_t	Velocity at Any Instant
Z	Induced Indentation Depth
E_t and E_s	Young's Modulus for Target and shot Material
v_t and v_s	Passion Ratio for Target and shot Material
a	Contact Radius

P_{max}	Maximum Pressure
σ_{ij}^{e} and σ_{ij}^{p}	Elastic and plastic Principal Stresses
σ_{eq}^{e} and σ_{eq}^{p}	Equivalent elastic and plastic Stress
s_{ij}^{e} and s_{ij}^{p}	Elastic and plastic Stress Deviations
σ_{m}^{e}	Mean Stress
ε_{eq}^{e} and ε_{eq}^{p}	Equivalent Elastic and plastic Strain
ε_{ij}^{e} and ε_{ij}^{p}	Elastic and plastic Principal Strain
e_{ij}^{e} and e_{ij}^{p}	Elastic and plastic Strain Deviations
σ_{s}	Yield Stress
β	Ratio of True Plastic Strain to Strain Exceeds Yield Strain
α	Hardening Coefficient
ε_{s}	Yield Strain
σ_{ij}^{r}	Residual Stress
ε_{ij}^{r}	Residual Strain
μ	Friction Coefficient
$\dot{\varepsilon}_{p}$ and $\dot{\varepsilon}_{o}$	Applied and Reference Strain Rate
T, T_{o} and T_{melt}	Applied, reference and melting Temperatures, respectively
A	Material Initial Yield Strength
B and n	Work Hardening Modulus and Exponent, Respectively
C and m	Strain Rate Sensitivity and Thermal Softing Coefficient, Respectively

Abbreviations

SP	Shot Peening
FEM	Finite Element Method
FEA	Finite Element Analysis
XRD	X-Ray Diffraction
CRSF	Compressive Residual Stress Field
CRS	Compressive Residual Stress
FE	Finite Element
3D	Three-Dimensional
DEM	Discreate Element Method
HRC	Rockwell Hardness
MCRS	Maximum Residual Compressive Stress
SCRS	Surface Residual Compressive Stress
CRS	Compressive Residual Stress
CRSL	Compressive Residual Stress Layer
AISI	American Iron and Steel Institute
RS	Residual Stress
CAE	Complete Abaqus Environment
CFD	Computational Fluid Dynamics
CAD	Computer Aided Design

Chapter One: Introduction

1.1. General

A lot of engineering components are subjected to high stress such as springs, wheels, turbine parts (blades, shafts), marine propellers, aircraft wings, internal combustion engine parts (valves, gears, crankshafts, connecting rods, pistons, cylinder heads). On such components, often safety is crucial since they are subjected to very high stress cycles in their operation period. In such cases, crack propagation is fast, and the time between crack initiation and total failure may only be minutes or hours of operation i.e. catastrophic and hence it is not possible to achieve high reliability by inspection or monitoring crack growth. One way of achieving high structural quality is to increase the fatigue strength of the component above the local fatigue stress. A very effective way for increasing fatigue strength is to modify the outermost surface component stress by shot peening [1,2].

Shot Peening (SP) is common industrial cold working process that is applied to induce a Compressive Residual Stresses field (CRSF) on the surface of a metallic component. In addition to CRSF shot peening refine the grain size and improve the microhardness (strain Harding) of material. Compressive stresses are beneficial in increasing resistance to fatigue failures (approximately by 30%), corrosion fatigue, fretting, wear. Shot peening may increase the component life by 500-1000% [3]. During the process, a large number of small spherical particles (0.2–2 mm), the so called ‘shots’, at high velocities strike the treated surface Figure 1.1. illustrates the shot peening process. Each shot acts as a small peen hammer, causing the surface to yield in plastic deformation and leaving a concave depression, termed dimple, on the surface of the target component. The stress field of the depression is similar to the field of a flat bar being bent. The concave side of the bar is in compression and the convex side is in tension. The normal stress along the cross section of the bar varies from a maximum compressive stress on the concave surface, to zero stress at the neutral axis up to a maximum tensile stress on the convex surface [2, 4-7].

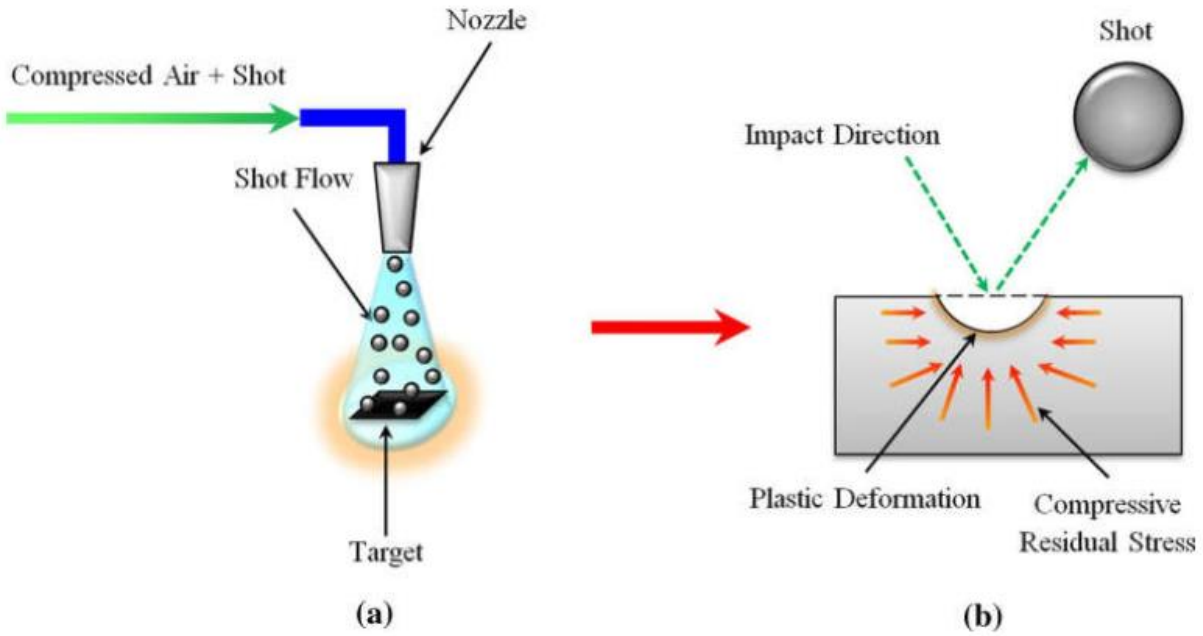

Figure 1.1. Schematic of shot peening process [7].

shot peening is a very complicated process to model and analyze, involving dynamic analysis of fast-moving shot striking on a metallic substrate/surface which can often has complex geometry [1,8-9]. There are a large number of parameters involved in shot peening process. These parameters can be categorized into three groups relating to the shot, the target and the process. intensity and coverage are the main parameters which determined the effectiveness of the shot peening process [10]. intensity is an indirect method to determine the amount of energy transferred to the surface of the Almen strip from the shot stream. Coverage is the percentage of area impacted by the shot peening process. So as to control the resulting residual stress distribution in shot peened substrate, it would be highly crucial to establish a relationship between these parameters and residual stress characteristics [1,4,10-11]. researches have been conducted to study shot peening experimentally [2, 12]. In spite of its effectiveness, the experimental method endures from several challenges related to the cost of experiments, time, and destructiveness [2,12]. Also, the majority of the experimental studies have used specific target so it is not easy to assimilate the effect of each parameter on the resulting residual stress distribution from the results [1]. To avoid experimental challenges, other researchers have proposed to study analytically the CRS in the peening component using Hertz contact and elastic-plastic theories [2]. Compared to experiments, the analytical method is much less

expensive. Can predict the residual stress distribution and the plastically deformed region in single shot impacts on components. Because of the complexity of the shot peening process, simplifying assumptions were adopted. These assumptions make these analytic approaches unsuitable for dealing with practical applications [13,2].

In Recent years, due to the increasing of computer power, numerical simulation using the Finite Element Method (FEM) software such as ABAQUS, ANSYS/LS-DYNA etc., has become an effective method to model the shot peening process and predict induced residual stresses. The numerical simulation is emphasized because of its advantages in efficiency and cost. A number of authors [1,2,9,10,13,14,20,22] conducted shot peening using the finite element method. 3D SP models have become the main choice, especially 3D models with dynamic analysis. The dynamic impact of a shot with high velocity and the double non-linearity of the problem due to the contact of two bodies and the elastic–plastic behavior of the target can all be taken in to account in an appropriate FE analysis [1,14]. However, there are only limited number of studies on the effect of surface pretreatments such as carburizing, on the residual stress distribution due to shot peening [28,39,68]. These surface pretreatments develop initial residual stress on the components to be peened and need further clarification. Besides, in realistic shot peening process, the number of shots are very high, but in existed numerical models used limited number of shots. in this paper, which is based on a pervious experiment [5]. The residual stress distribution introduced by multiple shots in the deformed surface layer of carburized Fe-0.85Mo-0.35C and Fe-1.5Mo-0.3C steel materials were investigated using ABAQUS/Explicit solver. First the compressive residual stress profile obtained from the experiment compared with the result determined from numerical analysis. Then Using FE modelling, a parametric study is also conducted to predict the effect of key parameters such as shot velocity, shot diameter, initial stress, and coverage on the distribution of residual stress and plastic deformation within the carburized target.

1.2. Problem Statement

So as to increase fatigue life, resistance to corrosion, microhardness, and prevent crack development and propagation of metallic components, shot peening is manly used in automotive and aeronautic industries. During the process a large number of small shots impact a metallic surface at high velocities. Its beneficial effects are mainly due to the residual stress field caused by the local plastic deformation of the near-surface region resulting from multiple shot impacts. Many researchers have been investigated the effect of various factors on the residual stress distribution induced by shot peening. However, there are only limited number of studies conducted on the effect of pretreatments such as carburizing, on the residual stress distribution and not yet clarified. The experimental method of determining residual stress has limitation regarding to time, cost and destructiveness. This paper presents the distribution of residual stress due to multiple shots impacting on carburized Fe-0.85Mo-0.35C and Fe-1.5Mo-0.3C steels by considering the effect of initial residual stress induced due to carburizing using a 3D finite element dynamic analysis. A program ABAQUS/Explicit was used as a modeling and analysis software. So numerical methods have to be used to predicate the distribution of residual stress in a material.

1.3. Objective

1.3.1. General Objective

The main and general objective of this study is numerical modeling of the residual Stress induced by multi-impact Shot Peening process on Carburized Fe-0.85Mo-0.35C and Fe-1.5Mo-0.3C Steel Materials

1.3.2. Specific Objective

- To model the ceramic shot peening process on a carburized prealloyed steels, via finite element analysis (FEA) using ABAQUS/Explicit 2020 software, to simulate the shot peening process and predict residual stress.
- To Study the effect of key parameters such as shot velocity, shot diameter, initial stress, and coverage on the distribution of residual stress (parametric study).
- To validate the numerical residual stress distribution with pervious experimental results.
- To investigate the effect of compressive residual stress, due to shot peening on the properties of carburized Fe-0.85Mo-0.35C and Fe-1.5Mo-0.3C steel materials.

1.4. Scope and limitation of the Study

1.4.1. Scope of the Study

The scope of this paper is just to investigate the residual stress distribution induced by shot peening in carburized Fe-0.85Mo-0.35C and Fe-1.5Mo-0.3C steel materials, using the 3D FEM dynamic analysis approach. Compared the numerical result with the experimental result [5]. The influence of key parameters such as peening velocity, shot diameter, initial stress and coverage have been investigated. But this work will not consider other parameters such as, peening time, mass flowrate, impact angle, etc.

1.4.2. Limitations

The carburized prealloyed steels are high strength materials and consists of elastic and plastic properties. The stress – strain characteristics of these materials is variable along the depth. However, in this study, it is assumed to be isotropic material properties. Since, shot peening is a surface treatment process and most often focused on the outer most surface region. SP is a cold working process. Thus, plastic deformation of the carburized prealloyed steel materials is independent of temperature. Besides, the surface roughness of the workpiece, which is the target material for the peening process, is also neglected. The simulated result cannot give exact result with the experiment, because peening parameters such as shot velocity, flow rate, diameter of shot, peening time etc. are deemed for commercial purpose and are not given for this study, while these parameters are the crucial input for FEA simulation and influence the residual stress result significantly.

1.5. Significance of the Study

The main significance of this paper is to examine whether the numerical model for shot peening results in similar residual stresses in trend compared to the experimental results or not. Also, the proposed model is used to identify the influence of shot peening parameters such as shot velocity, diameter, initial stress and coverage on the residual stress distribution and investigate the positive impact of shot peening on a carburized prealloyed steels.

1.6. Reliability, Validity and Objectivity

So as to achieve a valid and realistic result it is important to use proper simulation software and theory. In this study, A 3D FEM approach is used as a simulation software and the hertz contact theory as a proper theory have been used. Furthermore, this study uses pervious experimental data of [5] as a basis to assess the reliability and validity of the results. It can be said that the proposed model is valid and reliable if the outcome of this study is similar in trends to the results obtained from the experimental peening process presented.

1.7. Structure of the Thesis

The entire research work presented in this thesis can be covered by five chapters, as detailed below.

Chapter 1 is an introduction to this research, indicating the problem statement, objectives of this research, scope, limitation, and significance of the study as well as the outline of this thesis.

Chapter 2 covers an extensive literature review of the fundamentals and basic concepts of shot peening surface treatment, as well as the history, development of shot peening technique and theoretical background.

Chapter 3 describes the mechanical properties of target and shot materials. As well as the FEA simulation procedures for the peening process using Abaqus package.

Chapter 4 present the associated simulation result. Analyses of the residual stress variations along the depth of the surface layer extracted and compared with the experimental result. Besides, different shot peening parameters discussed here.

Chapter 5 conclusions and recommendation drawn from this research. Finally set future work.

Chapter Two: Literature Review

2.1. History of Shot Peeing Process

The method of increasing the strength of a metal began during ancient artisans and blacksmiths when they utilize a hammer to form different shape and enhance the strength of the armors date back to 2700 BC [15,16]. Figure 2.1 show a gold helmet, showing evidence of the process, is dated circa 2700 B.C. Before shot peening is modern practice blacksmith and sword makers were knowing the importance of shot peening. Nevertheless, it took thousands of years to understood the technique and combine with modernization. The current shot peening method was introduced in 1920's [10,15,16], by using metal, ceramic and glass shots. However, shot peening highly used during manufacturing throughout the Second World War era, with applications including the enhancement of the fatigue life on components such as leaf springs, connecting rods, crankshafts, camshafts, and aircraft landing gear structure [15]. Small amount of energy is transferred to the target, dynamically during shot peening by small metallic shots. The energy transferred to the target develops plastic deformation and residual stress at and under the peened target. Contact mechanics provides the necessary tools to develop the stress field in contacting objects. For the last 40 years shot peening got theoretical attention due to the development of several plasticity theories. Plasticity theory is crucial to estimate when the material yield [16].

Figure 2.1. An early example of cold working, a gold helmet [16].

The first shot peening machine was developed in 1927 by E.G. Herbert called the Cloudburst Machine, which thrown steel balls from a specific height on a target surface. There was a large amount of study conducted for work Harding of material by repeated bombardment of a spherical object. The desire of strongest materials during the second world war II increased the development of shot peening [16]. Almen strip and almen Gage were invented in 1943 by J.O. Almen. These strips are utilized to qualifying the shot peening process. Almen strips are thin strips shown in figure 2.2(a) of SAE1070 steel with different thickness used measure the intensity of a shot peening process. There are three types of strips and all strips are made from cold rolled spring steel tempered to 44 - 50 HRC and hot pressed for two hours to remove any residual stresses that may be present [16,10].

Almen strips that are smaller in thickness (0.03 inch) called N type strips, are used for lower intensities and thicker strips (0.094 inch) known as C type strips, are used for higher intensity levels. An intermediate intensity is used with A type strips of thickness 0.051 inch. Figure 2.2(c) shows the Almen gage, is a device used to measure Almen height that has been developed in the Almen strip by the shot induced compressive residual layer. This is easy application and a non-destructive test and the most common method to measure the intensity of the shot peening process. X-ray diffraction technique is the first method applied to measure the compressive residual stress induced by shot peening by E.W. Milburn. X-Ray diffraction and Almen test method made it possible to relate the intensity to the residual stress induced by shot peening process [10,15,16,11].

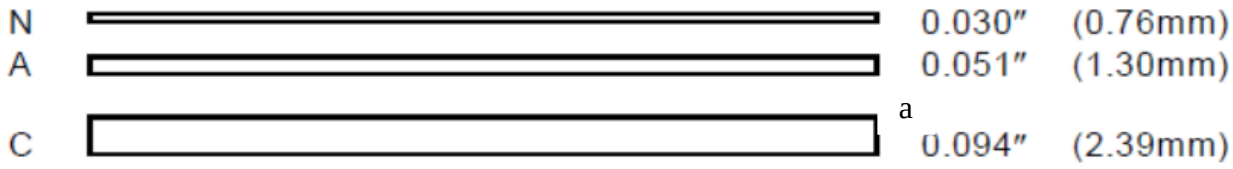

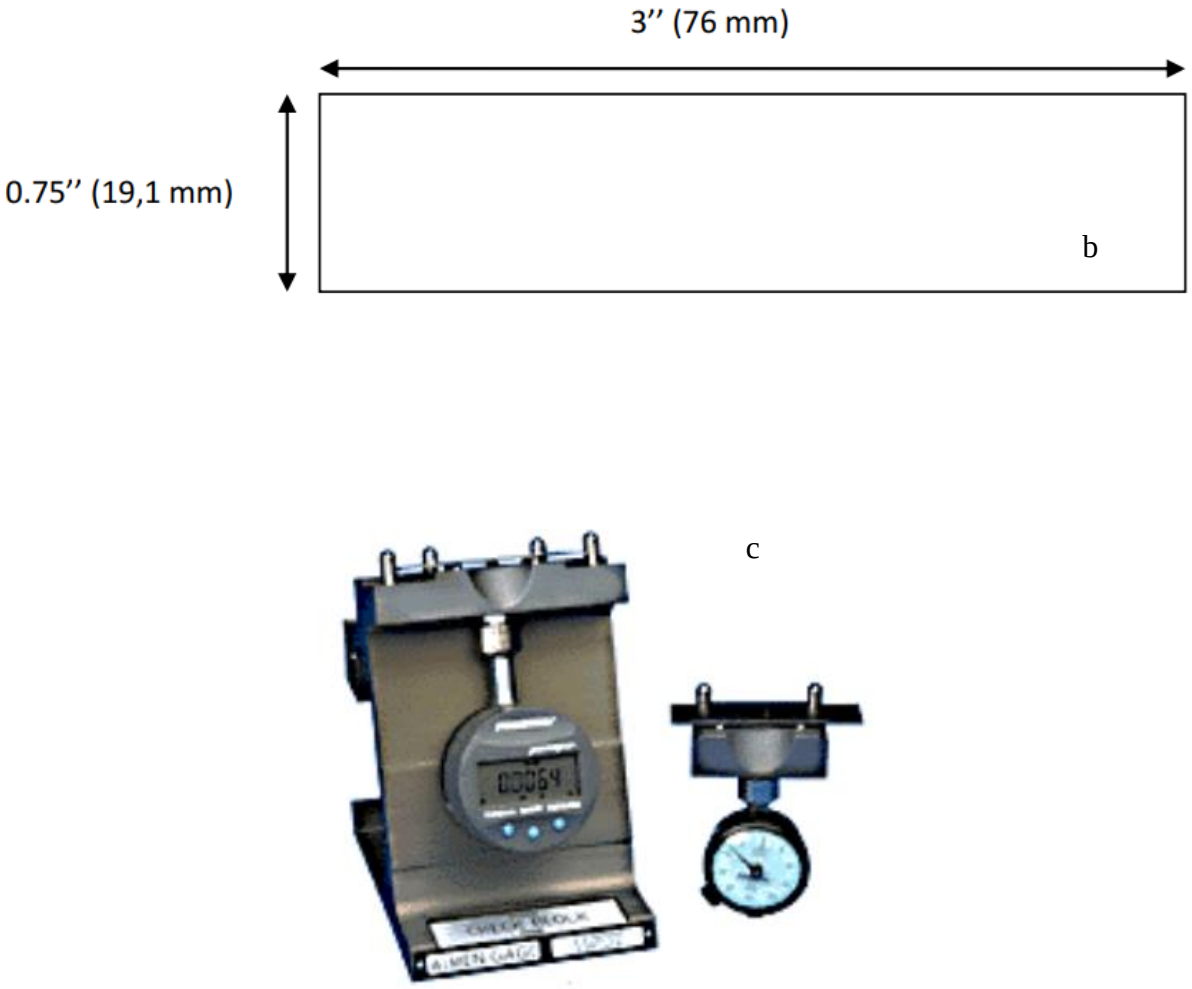

Figure 2.2. (a) Almen strips, (b) dimension of Almen strips, and (c) almen gage [11].

2.1.1. Shot Media

The amount of local plastic deformation on the surface and depth of compressive residual stress at the surface and subsurface are influenced by the type of shot media [11]. So as to have perfect collision between the shot and the substrate shot would comprise perfectly spherical particles, all of identical diameter, having infinitely high hardness, and fracture resistance [15]. Thus, it is very crucial to select the proper shot media in order to get the required compressive residual stress. The most common shot medias are ceramics, glass, or steel.

Figure 2.3. Shot medias ceramic, steel, and glass, respectively [17,18,19].

2.1.2. Shot Peening System

Shot peening is performed by propelled single or multiple tiny spherically shaped media at surface of a workpiece with high velocities. Each tiny spherical media that strikes the material acts as a peening hammer, imparting to the surface a small plastic indentation surrounded by a plastic zone. After the contact between the shot and the target ended, the elastically stressed component tends to recover to the original unloaded state, whereas the plastically deformed component develops permanent deformation on the surface of the work piece. These non-homogenous elasto-plastic deformations result in the development of a compressive residual stress field. The compressive residual stress layer developed in the surface of a work piece reduce premature failure and crack initiation of the metal component due to cyclic loading. [20,10,16]. Figure 2.4 shows an air-blast shot peening machine. The shots accelerate via air compressor system and impact the target component. The shots are return to the system after peening for repeating the process.

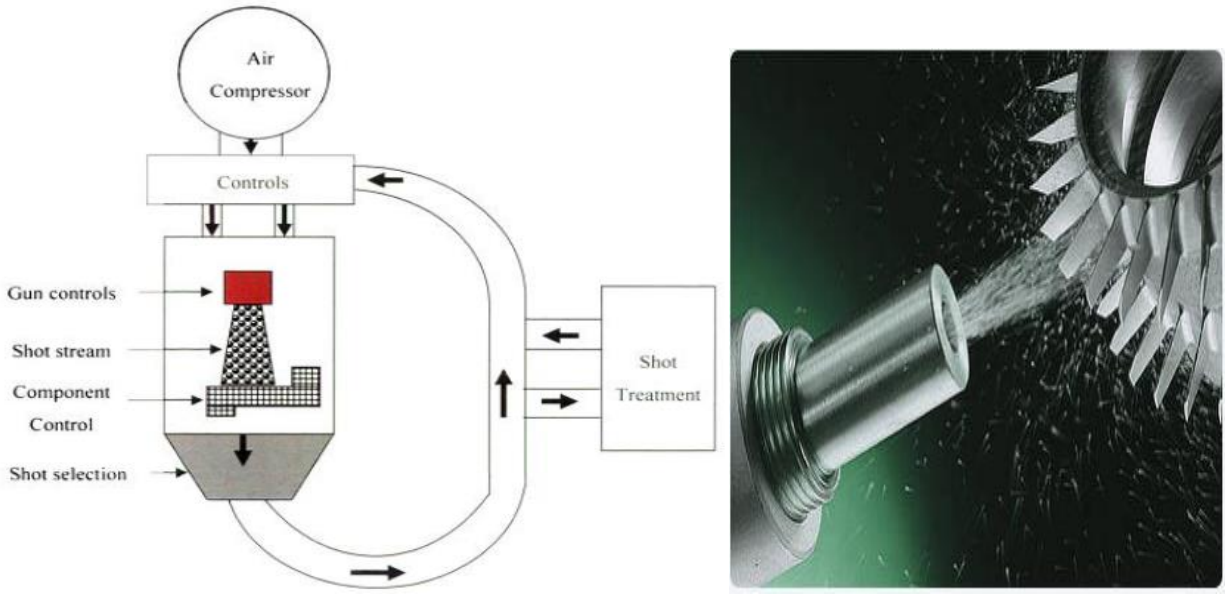

Figure 2.4. Schematic of shot peening equipment [10,21].

2.2. Shot Peening Parameters

The shot peening parameters must be controlled in order to get optimum benefit. a large number of parameters involved as shown figure 2.5 and it is difficult to control all the shot peening parameters in industry. However, there are two outputs which used to control the operating process, intensity and coverage [10,22]. Media. Size, media shape, media hardness, shot flow rate, shot velocity, nozzle-workpiece distance and impact angle are parameters which directly affect the intensity. Whereas the coverage in influenced by parameters such as a system type (nozzle or wheel), nozzle geometry, shot velocity, angle of impact, mass flow rate, shot peening time, shot peening media and properties of the workpiece.

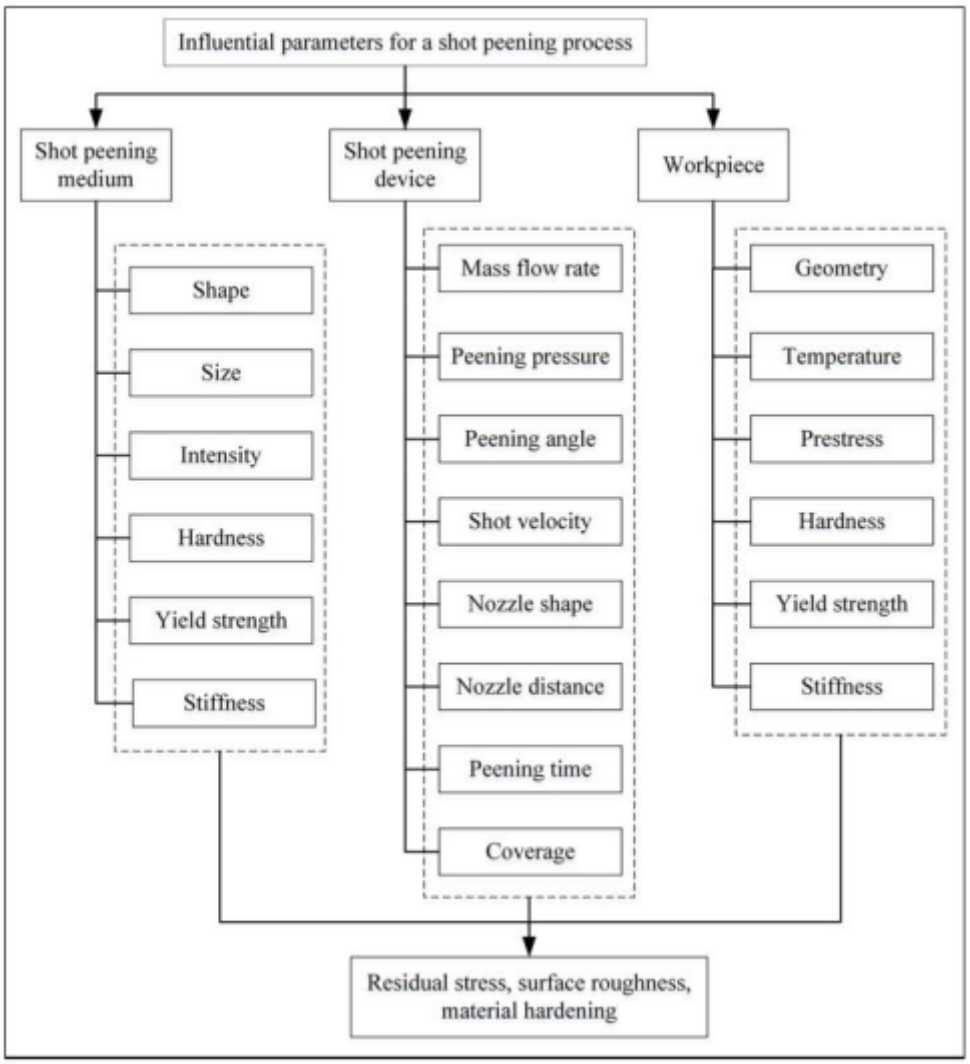

Figure 2.5. Influential parameters and product [23].

2.2.1. Intensity, Arc Height and Saturation

Intensity is a measure of the amount of energy transferred to the target material by shot particles. The Almen strip and Almen gage are tools used to measure the intensity of the shot stream. The intensity is proportional to the degree of curvature [24 ,16,10]. The intensity (energy) of a shot stream is a function of shot velocity, shot diameter and density of shots.

The Almen strip is mounted (Figure 2.6) in a holding fixture, and is peened at a specific condition. When a test strip is shot peened the strip will bend and a measurable arc develops, i.e. the strip will deflect into the shot stream. The deflection of the strip into the shot stream occurs

because the surface area of the peened side is increasing. Lastly, the arc height is measured by the Almen gage and plot it with the exposure time to draw the saturation curve.

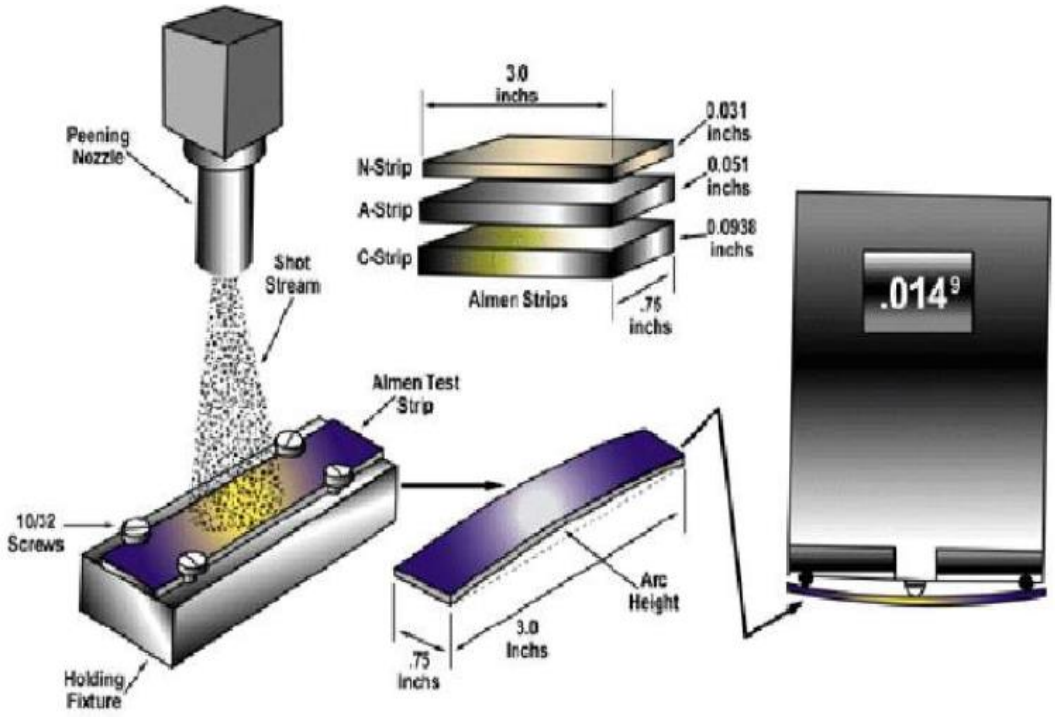

Figure 2.6. Almen's strips and intensity measurement procedure [25].

2.2.1.1. Saturation Curve

So as to obtain the intensity of the shot peening process. Almen strips are shot peened for a given period of time and its arc height is measured by the Almen gage after each time period. These measurements provide the maximum arc height at certain air pressure and mass flow rate. Consequently, saturation point of the operation can be found. Finally, saturation curve is obtained by plotting arc Hight Vs peened time (figure 2.7) [11]. Therefore, Saturation is a point on the curve, for which doubling the peening time increase the arc height no more than ten percent. T is the minimum time that meets the specification. Longer times than T would meet the specification as stated [10,11].

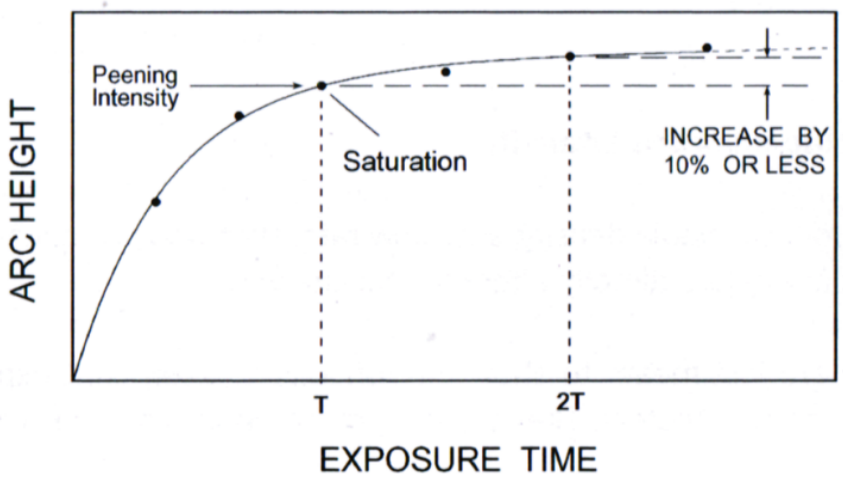

Figure 2.7. Saturation curve [10].

2.2.2. Coverage

Coverage is the percentage of exposed area which has been peened during a given period of time (figure 2.8 (a)). In many industrial applications, the range of coverage is from 100% to 200%, in which the residual stress is uniform and meet the required value and the surface is not damaged by the shot [16,10]. Coverage provides a direct way to tell if a target has been peened the necessary amount, not too little and not too much. When a target is highly peened the surface develops detrimental stress raisers such as folding sites and an excessively rough surface. These unacceptable surface characteristics create crack nucleation sites and can lead to premature failure of the component and therefore render shot peening a harmful surface treatment process. Conversely, when a target is under peened the beneficial compressive stress in the material is not developed enough to optimize the full benefits of peening and inhibits maximization of the lifetime of a given part. The method to determine coverage is through visual inspection [16,10]. Visual inspection is performed using a microscope or magnifying glass. A microscopic photograph of the surface can also be taken by image analysis software that is capable of accurately calculating the percent of peened area. The percentage of coverage increase with peening time up to certain limit [10]. Figure 2.8(b) shows an example of the variation of coverage with respect to peening time.

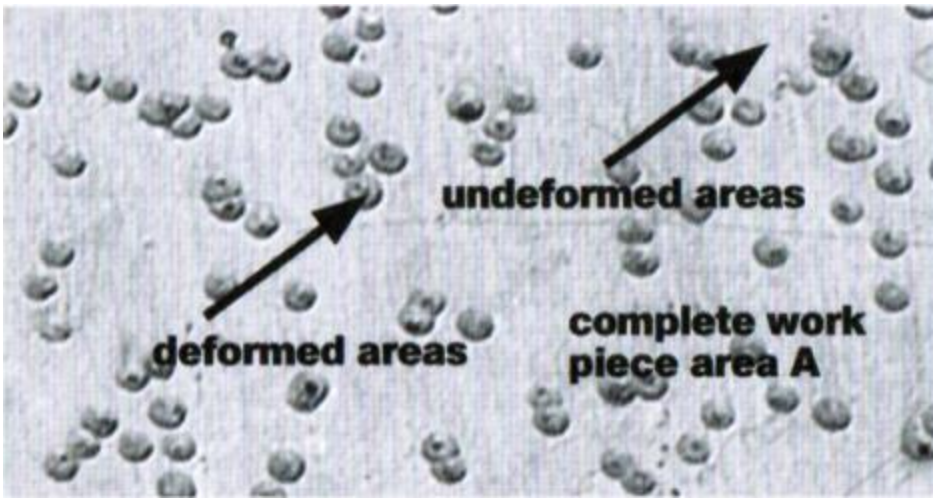

a

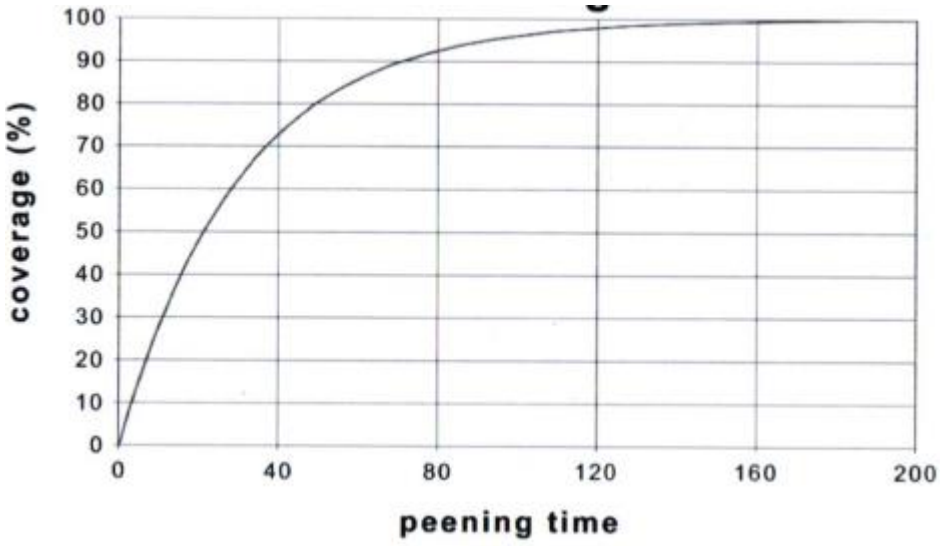

b

Figure 2.8. Coverage (a) definition and (b) as a function of time [10].

Kirk developed a theoretical model based on Avrami equation, to determine percentage of coverage which is [24,16,10]:

$$C_{(t)}=100\left[1-\exp\left(-\frac{3R^2\dot{m}t}{4Ar^3\rho_s}\right)\right]$$

where *C(t)* is the coverage at any particular time, *R* is the average radius of indentations caused by a single shot, $\dot{m}$ is mass flow rate of shot, *t* is exposure time, *A* is area of shot spread, *r* is the average radius of shot, ρ_s is the shot density.

2.3. Residual Stress

2.3.1. Overview of The Residual Stress

The important enhancement of a material, through the shot peening process is due to the induced compressive residual stress near surface [15]. [10] states there is no crack initiation and crack propagation on a component having compressive stress zone. Moreover, most often fatigue and stress corrosion failures start at or close to the surface. Shot peening increase the compressive residual stress up to 60% near the surface [16]. Thus, the induced compressive stress developed in a material due to shot peening has a significant important in terms of increasing the life of the mechanical components.

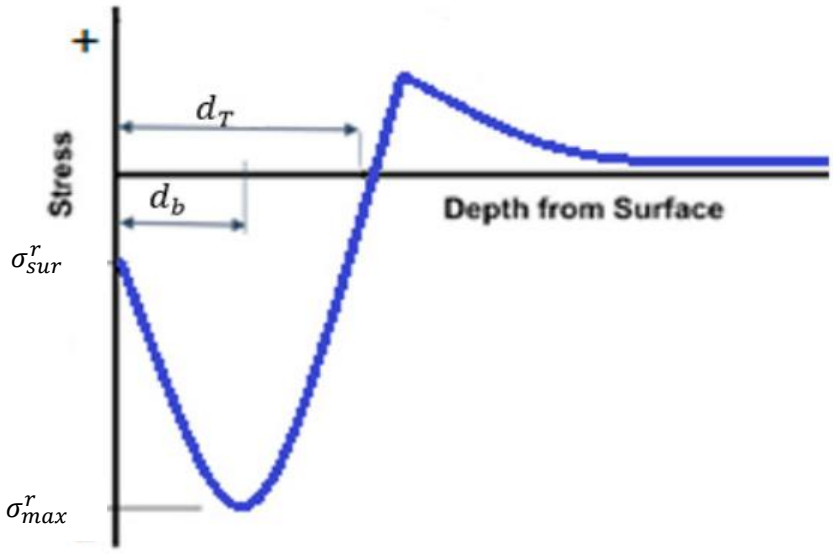

Figure 2.9. A typical residual stress profile due to shot peening [26].

Figure 2.9 shows a typical residual stress distribution in a material. it has been characterized by a surface compressive stress (σ^r_{sur}), a near-surface maximum compressive stress (σ^r_{max}) at a beneficial depth (d_b), a total depth (d_T) of compressive stress, and a tensile stress region in the remaining section of the depth from the treated surface. The distribution of the residual stress

influenced by work piece thickness, shot properties such as density, velocity, and hardness. A work piece having thin section experiences an increase in the tensile stress just after the total depth of compressive stress. A harder shot develops higher compressive residual stress near the surface of the material to be treated, as well as shots having higher velocity can produce both higher and deeper compressive stress, for enhanced fatigue life [26].

The effect of different shot peening parameters has been analyzed by Herzog et al. (1996). Figure 2.10 shows the influence of different shot peening parameters on the residual stress distribution of a material. In this figure, the directions of the arrows show the influence of these parameters on residual stress profile. Arrow 1 shows that the value of the surface residual stress σ_{sur}^{r} increases with the increase of HV_s and HV_m; arrow 2 shows that the value of the maximum residual stress σ_{max}^{r} increases with the increase of $V, p, d, t,\ HV_s$ and HV_m; arrow 3 shows that the depth of the maximum residual stress decreases with the increase of HV_m and arrow 4 shows that depth of CRSL increases with the increase of V, p, d, t,and HV_s[26].

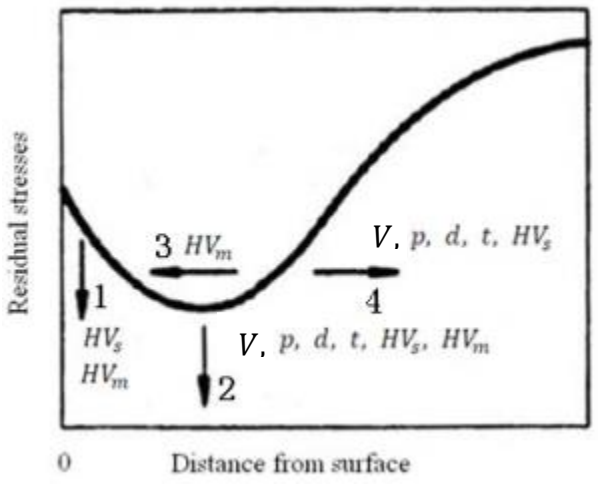

Figure 2.10. The effect of parameters on the residual stress profile [26].

2.3.2. Practical Residual Stress Measurement Methods

Residual stress is a “lock-in” stress that exist in a material after the removal of the load applied on it [10]. There are a number of methods to measure the residual stress developed in a material such as X-ray diffraction, Hole Drilling, Neutron Diffraction, Barkhausen Noise, Ultrasonic, Sectioning, Contour, Deep hole drilling, Synchrotron [10,24]. These methods are classified as destructive, semi-destructive and non-detective. Both the destructive and semi destructive

method are mechanical methods work based on material removal of material from the peened component or stress -relaxation. These methods measure deformations of the material when residual stresses releases during the material removal. The non-destructive method measures the residual stress by measuring some parameters related to the stress such as the interplanar spacing from their stress-free value. Then, the strain could be analyzed by applying Bragg's law. However, x-ray diffraction (XRD) methods is the most widely accepted nondestructive methods for measuring residual stresses of peened components, due to its easy and relatively accurate results [10].

2.3.2.1. X-Ray Diffraction Measurement Technique

In order to determine the residual stress in a material using x-ray diffraction (XRD) method, first the strain in the crystal lattice is measured, then from the measured strain and the material elastic constants the residual stress can be obtained. However, it measures near surface residual stress. X-ray diffractometer consists of x-ray source (S), a detector(D). the x-ray source(S) focused on the sample material and emits beam of rays (in known orientation) and then diffracted based upon the orientation of the material polycrystalline lattice. x-ray detector (D) sense the diffracted x-rays. The diffraction angle (2θ) is the angle between the diffracted beam and the incident beam's subsurface trajectory. The angle psi (ψ) defines the orientation of the sample, and is the angle between the incident and diffracted beam bisector, and the normal of the surface (N) [15].

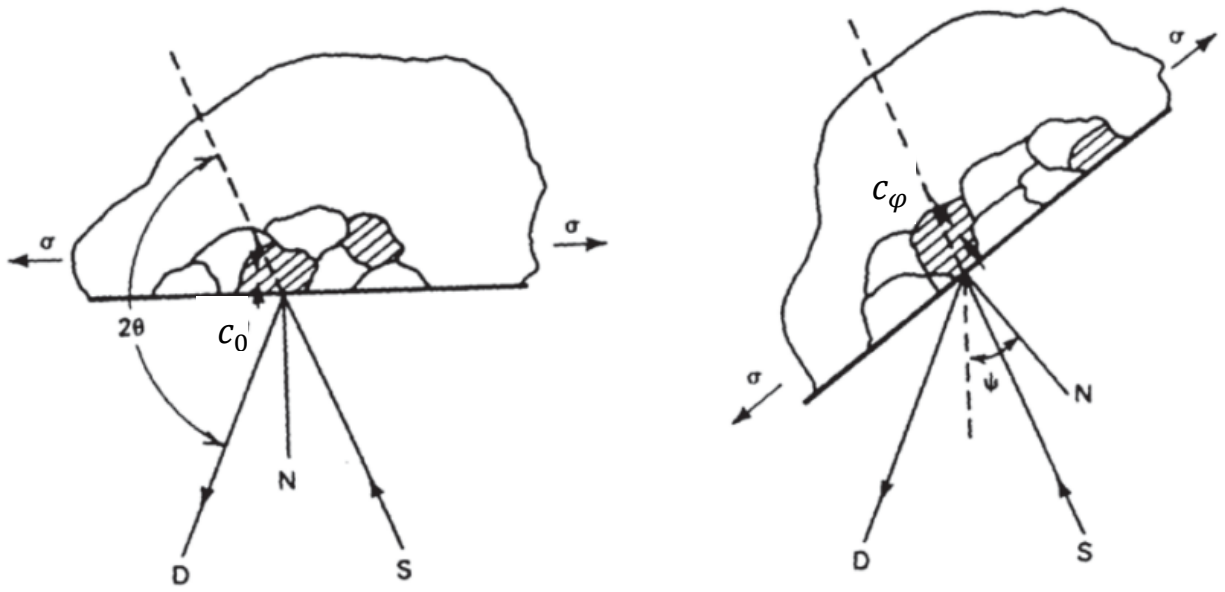

Figure 2.11. Schematic of x-ray diffraction's principle geometry, with (Left) sample at orientation ψ =0 and (Right) orientation ψ= ψ [15]

X-ray diffractometer works based on Bragg's Law, the diffraction angle (2θ) is dependent upon the crystalline lattice spacing of the sample, d. Subsequently, any change in c, results in a corresponding change to the measured diffraction angle. Measuring the change in in the angular position of the diffraction peak for at least two of the sample defined by the angle psi (ψ) allows the calculation of the residual stress present. in x-ray diffraction process, detects any changes in c. plastic deformation and dislocation occur in crystalline structure of material if any change in d greater than elastic. The residual stress obtained by x-ray diffraction method is a representative residual stress due to elastic strain on a macroscopic scale of which the x-ray beam is averaged over a volume. The residual stress can be calculated [15,11].

$$\sigma^r = \left(\frac{E_s}{1+v_s}\right) * \frac{1}{c_0}\left(\frac{\delta c_\varphi}{dsin\varphi^2}\right)$$

c_0= lattice spacing for unstressed material

c_φ= lattice spacing in the direction φ

Table 2.1 X-ray diffraction measurement conditions of residual stress for carburized steels after shot peened [5].

Incident Radiation	Cr Kα	Elementary Cell	Cubic
Filter	Vanadium	Miller's Index (hkl)	211
Diffractometer configuration	ω	Multi-regression	Yes
Detector type	30°	Background subtraction	Polynomial
Detector's angle range	Strip	2θ position	Free
Acquisition time	30 s	2θ angle	156.33°
Oscillation range	+/-40°	Young modulus	208000 MPa
Number of Ψ angles used	7	Poisson coefficient	0.28
Selection of Ψ	Automatic	Power supply	33 kV
Measurements method	Static	Current the tube's	85 µA
Materials	Steel	Collimator's diameter	1 mm

2.4. Analytical Model for Shot Peening Induced Residual Stress

Compressive residual stress develops in a material while the high-speed spherical shots collide with the substrate material. This phenomenon is analyzed using the motion equation of the shot, the Hertz theory of elastic contact, and the Ilyushin's simplified elasto-plastic theory. The main assumptions are as follows: [28,16,8].

i. Load at collision can be calculated by an elastic analysis in the case where a hard shot collides vertically with a target, as shown in Fig, a.
ii. The stress-strain relation of the target material is elasto-plastic, as shown in Fig. b.
iii. A minute element in a body receives loading and unloading of the Hertz stress field without any relation to the surroundings.
iv. The residual stress resulting from the transformation of retained austenite into martensite is not considered.
v. The influence of initial residual stress that exists after heat treatment is not considered.

vi. It is assumed that the shot-peened part (target material) is a semi finite body.

vii. A homogeneous residual stress field and associated plastic strain exist at any specified depth due to the assumption that a semi finite body has been uniformly loaded.

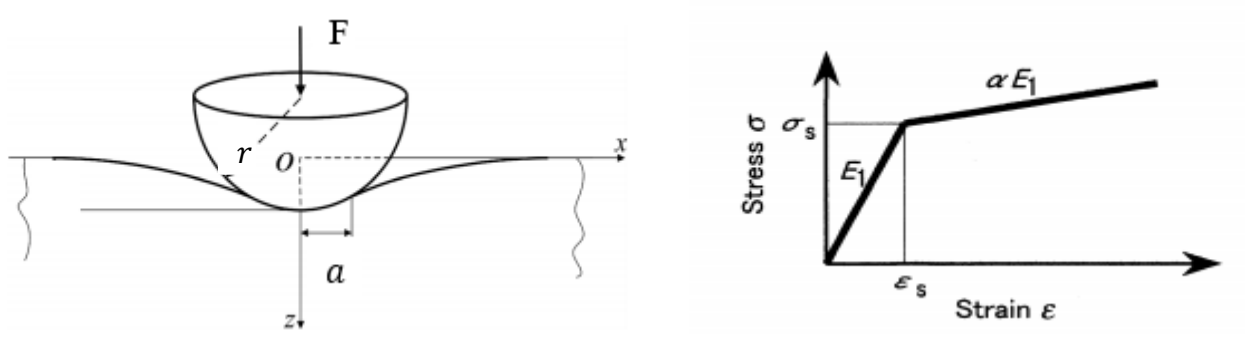

a b

Figure 2.12. a) Indentation of a rigid sphere on an elastic half b) Stress-strain relation of target material. [67]

2.4.1. Load and Stress During Collision by Elastic Analysis

Expressing the force acting on a shot at any instant during collision as F_t,the motion of a shot (density ρ_s , diameter d, velocity V_t) may be expressed by the equation

$$\frac{d}{dt}\left(\frac{1}{6}\pi d^3 \rho_s V_t\right) = F_t \quad \text{(1)}$$

Converting time t into the position of a shot on the z axis,

$$\frac{1}{6}\pi d^3 \rho_s V_t * dV_t = F_t * dz \quad \text{(2)}$$

Based on the Hertz theory of elastic contact, the mutual approach z of two bodies when a shot is pressed against a target in force F_t is as follows,

$$z = \left(\frac{9F_t^2}{8dE^{*2}}\right)^{1/3} \quad \text{(3)}$$

where z is induced indentation depth

$$\frac{1}{E^*} = \frac{1-v_t^2}{E_t} + \frac{1-v_s^2}{E_s} \quad \text{(4)}$$

Where E is the young's modulus and v is the passion ratio. Subscript 1 shows the target material, and Subscript 2 shows the shot. Substituting F_t from Eqs. (3) into Eqs. (2), and integrating from the beginning of the collision to the time at which the shot velocity is zero (initial velocity V and final load F), F is given by

$$F = \frac{1}{3}\left(\frac{5\pi}{4}\right)^{3/5} {\rho_s}^{3/5} d^2 {E^*}^{2/5} V^{6/5} \quad \text{..... (5)}$$

Based on the Hertz theory of elastic contact, when a shot is pressed against a target by the force F, the contact radius a and the maximum pressure P_{max} are given by

$$a = \left(\frac{3dF}{8E^*}\right)^{1/3} \quad \text{..... (6)}$$

$$P_{max} = \left(\frac{24E^{*2}F}{\pi^3 d^2}\right)^{1/3} \quad \text{..... (7)}$$

The principal stresses σ_x, σ_y, σ_z, the equivalent stress σ_{eq}, and the stress deviations s_x, s_y, s_z on the z-axis are given by Eqs. (8-11), marked by superscript e, as these are elastic calculations.

$$\sigma_x^e = \sigma_y^e = -P_{max}\left[(1+v_t)\left(1-\frac{z}{a}\tan^{-1}\left(\frac{a}{z}\right)\right)-\frac{1}{2}\left(1+\frac{z^2}{a^2}\right)^{-1}\right] \quad \text{.. (8)}$$

$$\sigma_z^e = -P_{max}\left(1+\frac{z^2}{a^2}\right)^{-1}$$

$$\sigma_{eq}^e = \frac{1}{\sqrt{2}}\left[\left(\sigma_x^e-\sigma_y^e\right)^2+\left(\sigma_y^e-\sigma_z^e\right)^2+\left(\sigma_z^e-\sigma_x^e\right)^2\right]^{1/2}$$

$$= P_{max}\left[\frac{3}{2}\left(1+\frac{z^2}{a^2}\right)^{-1}-(1+v_t)\left(1-\frac{z}{a}\tan^{-1}\left(\frac{a}{z}\right)\right)\right] \quad \text{..... (9)}$$

$$\sigma_m^e = \frac{1}{3}\left(\sigma_x^e+\sigma_y^e+\sigma_z^e\right) \quad \text{..... (10)}$$

Where σ_m^e,is the mean stress

σ_{eq}^e = von mises equivalent stress

$$s_x^e = s_y^e = \sigma_x^e - \sigma_m^e = \frac{1}{3}\sigma_{eq}^e \quad \text{..... (11)}$$

$$s_z^e = -\frac{2}{3}\sigma_{eq}^e$$

The equivalent strain ε_{eq}^{e} and the component strains ε_{x}^{e}, ε_{y}^{e}, ε_{z}^{e} are

$\varepsilon_{eq}^{e} = \frac{\sigma_{eq}^{e}}{E_1}$……..……..…... (12)

ε_{x}^{e}=$\varepsilon_{y}^{e} = \frac{1}{E_t}\left[\sigma_{x}^{e} - v_t(\sigma_{y}^{e} + \sigma_{z}^{e})\right]$

$$\varepsilon_{z}^{e} = \frac{1}{E_t}(\sigma_{z}^{e} - 2v_t\sigma_{x}^{e})$$

Mean strain can be written as

$$\varepsilon_{m}^{e} = \frac{1}{3}\left(\varepsilon_{x}^{e} + \varepsilon_{y}^{e} + \varepsilon_{z}^{e}\right)$$

From Eqs. (11) and (12), the strain deviations e_{x}^{e} , e_{y}^{e}, e_{z}^{e} are

e_{x}^{e} = $e_{y}^{e} = \frac{s_{x}^{e}}{E_t} = \frac{1}{3}(1 + v_t)\varepsilon_{eq}^{e}$…….……..… (13)

e_{Z}^{e} = $-2e_{x}^{e}$

Here, it is proved that the equivalent stress σ_{eq}^{e} on the z axis has a maximum value at $z = 0.48a$ from the numeric calculation of Eqs. (9). Thus, the following analysis is carried out, considering that the maximum compressive residual stress is generated at this position.

2.4.2. Compressive Residual Stress by Elastic-Plastic Analysis

2.4.2.1. Residual Stress After Collision of One Shot

First, the loading process during collision is considered. The σ-ε curve of the target material is simplified as shown in Fig. 2. The material hardens by inclination αE1 after exceeding the yield stress σ_s by the applied stress. To calculate the strain strictly in an elastic-plastic region is very complex. Therefore, it is simplified as follows using a coefficient β. β is the ratio of the true plastic strain to the strain in the part that exceeds the yield strain ε_s in the apparent elastic strain ε_{eq}^{e} calculated by Eq. (12). Superscript e here shows an elastic calculation, and superscript p shows an elasto-plastic calculation.

$$\varepsilon_{eq}^{p} = \varepsilon_{eq}^{e} \quad For\ \varepsilon_{eq}^{e} \leq \varepsilon_s$$

$\varepsilon_{eq}^{p} = \varepsilon_s + \beta\left(\varepsilon_{eq}^{e} - \varepsilon_s\right) \quad For\ \varepsilon_{eq}^{e} > \varepsilon_s$……..…….. (14)

From the σ-ε curve, σ_{eq}^{p} is expressed by

$$\sigma_{eq}^{p} = \sigma_{eq}^{e} \qquad for\ \varepsilon_{eq}^{e} \le \varepsilon_s$$

$\sigma_{eq}^{p} = \sigma_s + \alpha E_t\left(\varepsilon_{eq}^{p} - \varepsilon_s\right) \qquad for\ \varepsilon_{eq}^{p} > \varepsilon_s$…… (15)

When it is thought that the Eq. (13) is appropriate in an elasto-plastic area, the next equation is obtained.

$e_x^p = e_y^p = \frac{1}{3}(1 + v_t)\varepsilon_{eq}^{p}, \qquad e_Z^p = -2e_x^p$……..…… (16)

Moreover, when the equivalent strain ε_{eq}^{p} is taken to agree with the tension strain at axial tension and the Ilyushin's elasto-plastic theory is used, the relation between the stress deviation s_{ij}^{p} and the strain deviation e_{ij}^{p} in the plastic region of minute strain is given by

$s_{ij}^{P} = \frac{1}{1+v_t}\frac{\sigma_{eq}^{p}}{\varepsilon_{eq}^{p}} e_{ij}^{P}$……..…….. (17)

Substituting Eq. (16) for Eq. (17),

$s_x^P = s_y^P = \frac{1}{1+v_t}\frac{\sigma_{eq}^{p}}{\varepsilon_{eq}^{p}} e_x^P = \frac{1}{3}\sigma_{eq}^{p}$……..…… (18)

$$s_z^P = -2s_x^P$$

The stress and the strain in the loading process are calculated as above. Next, the unloading process and the residual stress are considered. When assuming the deformation behavior of the material is isotropic at unloading and the deformation is small, the stress after unloading is

$$\sigma_{ij}^{r} = s_{ij}^{P} - s_{ij}^{e}$$

where superscript r shows to be a state after unloading. When expressed by the principal stresses using Eq. (18),

$$\sigma_x^r = \sigma_y^r = \sigma_z^r = 0 \qquad for\ \sigma_{eq}^{e} \le \sigma_s$$

$\sigma_x^r = \sigma_y^r = \frac{1}{3}\left(\sigma_{eq}^{P} - \sigma_{eq}^{e}\right) \qquad for\ \sigma_s < \sigma_{eq}^{e} \le 2\sigma_{eq}^{p}$…… (19)

When σ_{eq}^{e}>$2\sigma_{eq}^{p}$, yielding and hardening must take place in the unloading process. Therefore,

$$\sigma_{\mathrm{x}}^{\mathrm{r}} = \sigma_{\mathrm{y}}^{\mathrm{r}} = \frac{1}{3}\left(\sigma_{eq}^{P} - 2\sigma_{eq}^{p} - \Delta\sigma_{eq}^{P}\right)$$

$$= \frac{1}{3}\left(\sigma_{eq}^{P} - 2\sigma_{eq}^{p} - \alpha\beta(\sigma_{eq}^{e} - 2\sigma_{eq}^{p})\right) \ldots\ldots\ldots\ldots\ldots\ldots\ldots\ldots\ldots\ldots \text{(20)}$$

$\sigma_{\mathrm{z}}^{\mathrm{r}}$=-2$\sigma_{\mathrm{x}}^{\mathrm{r}}$

The maximum compressive residual stress after one shot has collided with a target and has rebounded can be calculated by Equation (19) and (20).

2.4.2.2. Residual Stress in Full Coverage

The residual stress after enough shots have collided so that the coverage reached 100% or more is considered. From the boundary condition,$\sigma_{\mathrm{z}}^{\mathrm{r}} = 0$ at z=0. moreover, the plastic deformation after shot peening at 100% coverage may be uniform and continuous in the x-y plane. Therefore $\varepsilon_x^r = \varepsilon_y^r = 0$ and $\sigma_{\mathrm{z}}^{\mathrm{r}} = 0$.thus , if $\sigma_{\mathrm{z}}^{\mathrm{r}}$ is completely relaxed, the variation $\Delta\sigma_{\mathrm{x}}^{\mathrm{r}}$of $\sigma_{\mathrm{x}}^{\mathrm{r}}$, the variation$\Delta\sigma_{\mathrm{y}}^{\mathrm{r}}$ of $\sigma_{\mathrm{y}}^{\mathrm{r}}$, and maximum compressive residual stress $\sigma_{\mathrm{max}}^{\mathrm{r}}$finally generated are as follows. When the yield does not happen by the relaxation process, these are

$$\Delta\sigma_{\mathrm{x}}^{\mathrm{r}} = \Delta\sigma_{\mathrm{y}}^{\mathrm{r}} = -\frac{v_t}{1 - v_t}\sigma_{\mathrm{z}}^{\mathrm{r}}$$

$\sigma_{\mathrm{max}}^{\mathrm{r}} = \sigma_{\mathrm{x}}^{\mathrm{r}} - \frac{v_t}{1-v_t}\sigma_{\mathrm{z}}^{\mathrm{r}} = \frac{1+v_t}{1-v_t}\sigma_{\mathrm{x}}^{\mathrm{r}}$ ……... (21)

when the yield happens by the relaxation process, these are

$$\Delta\sigma_{\mathrm{x}}^{\mathrm{r}} = \Delta\sigma_{\mathrm{y}}^{\mathrm{r}} = -\frac{\alpha\beta v_t}{1 - v_t}\sigma_{\mathrm{z}}^{\mathrm{r}}$$

$\sigma_{\mathrm{max}}^{\mathrm{r}} = \sigma_{\mathrm{x}}^{\mathrm{r}} - \frac{\alpha\beta v_t}{1-v_t}\sigma_{\mathrm{z}}^{\mathrm{r}} = \frac{1-v_t+2\alpha\beta v_t}{1-v_t}\sigma_{\mathrm{x}}^{\mathrm{r}}$ …….. (22)

moreover, modifying Eqs (21) and (22) using Eqs. (6), (7), (19) and (20) as $v_t = 0.3$, the maximum compressive residual stress $\sigma_{\mathrm{max}}^{\mathrm{r}}$ is represented by using the shot peening condition as variables. When the yield does not happen by the unloading process,

$\sigma_{\mathrm{max}}^{\mathrm{r}} = 0.619(1 - \alpha\beta)(\sigma_s - 0.519{\rho_S}^{1/5}{E^*}^{4/5}V^{2/5})$ ……..…. (23)

when the yield happens by the unloading process,

$$\sigma_{\max}^{r} = (0.333 + 0.286\alpha\beta)(1 - \alpha\beta)$$

$[(2\alpha\beta - 1)\sigma_s - 1.038\alpha\beta{\rho_S}^{1/5}{E^*}^{4/5}V^{2/5}]$ …….…….. (24)

The maximum compressive residual stress produced by shot peening can be predicated from the shot peening conditions and the material characteristics using Eqs. (23) or (24).

2.4.3. Calculating Peak Depth of Residual Stress

From the basic assumptions described above, the predicted peak depth d_b, of the maximum compressive residual stress coincides with the depth where the equivalent stress σ_{eq}^{e} calculated based on the Hertz theory of elastic contact is at its maximum. That is,

$$d_b = 0.48a$$

$= 0.316{\rho}^{1/5}d{E^*}^{-1/5}V^{2/5}$……..…….. (25)

2.5. Existed Research Survey

A good understanding regarding to shot peening process is very crucial since it has remarkable importance to increase fatigue resistance, increase corrosion resistance, lubrication and tribological application, and surface Nano crystallization. It is used in industries such as automotive, aerospace, nuclear, medical, pressure vessel and petroleum. Shot peening prevent fatigue failure through two mechanisms:

1.) by inducing a compressive residual stress on the target material which prevent crack growth a

2.) enhancing the material hardness that prevent crack initiation.

A compressive residual stress is a stress that stays in a component, at equilibrium, after all external loads have been removed [29]. Due to all the above uses and applications, many scholars have been studied the distribution of residual stress induced on the peened material using different models. For instance:

Hong et al. [13], used a single-shot impact on a metallic component to study the effects of the various peening parameters such as shot diameter, impact velocity, incident angle, initial yield stress, and Hardening constant, on the residual stress distribution using 3D finite element dynamic analysis. They reported that the shot diameter has a negligible effect on the magnitude of SCRS and MCRS, but depth of RS zone increases linearly with increasing shot diameter. Increasing impact velocity do not have influence on SCRS and MCRS for perfectly plastic material, but has significant effect for plastic strain hardening material. Also, for perfectly plastic material RS increases linearly as yield stress increase. Effect of strain hardening is much complex its effect depends on strain hardening yield stress to the initial yield stress and the impact energy.

Mahmoudi et al. [30] studied the effect of initial surface treatment on the distribution of residual stress, analytically with experimental verification. They concluded any initial stress found in a material can be wiped out while the material shot peened up to the maximum compressive residual stress point. However, beyond the maximum point the shot peening residual stresses dramatically alter. Besides rough grinding before shot peening not only generated high compressive residual stress but also increased surface hardness. The simulation result was in good agreement with the experimental.

Lechun Xie et al. [14] investigated the variation of residual stress using 3D FE dynamic simulation on titanium matrix composite. Concluded increasing coverage rate while keeping the velocity constant, the CRS layer remain constant but the MCRS change significantly. But as the velocity increase 50m/s to 100m/s parallel with coverage rate both SCRS and MCRS significantly increases. When the velocity of the shot ball is 100m/s, the maximum residual stress no longer increases even after the SP coverage rate increase. This result indicates that once the impact effect on material reaches a certain level, the residual stress Field vary only slightly, and finally these values can be considered as the saturation values.

Mylonas et al. [31], simulated shot peening process using a 3D FE model that consists of elastic plastic target and rigid sphere. Also, investigated the influence of different parameters such as shot velocity, incident angle and diameter on the induced RS. The MCRS is increasing with increasing shot velocity for all cases. the MCRS is increasing when a larger shot is used. It is also clear that for the same shot size, the effect of impinging angle on the RS magnitude is

insignificant. The depth of residual stress layer increases when velocity and diameter of shot increases.

Qinjie Lin et al. [32], investigated the influence of peening velocity, coverage, and doubling peening on the surface integrity of a substrate using 3D FEM. Found that increasing peening velocity (shot peening intensity) is a best way of obtaining finer and deeper microstructure on the material. However, it increases the surface roughness. And also, the higher velocity creates thicker CRSL and deeper MCRS. Coverage does not have that Mach effect compared to the velocity but it increases the MCRS gradually. neither increasing the peening velocity nor coverage can increase the SCRS. To fill this gap, double peening technique provides a potential alternative way.

Meguid et al. [33], conducted 3D FEM dynamic simulation on strain sensitive target. Multi impact shot peening provide uniform residual stress on the material than single impact. Proper separation between consecutive shots has significant effect on the distribution of residual stress. So as to produce stable residual stress distribution the vertical distance between each shot could be sufficient to recover the target component before the next shot is impacted.

Manoucherifar et al. [34], using a comprehensive 3D finite element dynamic analysis with consideration of the spring-back effect was conducted to simulate the shot peening process.in this work they found, increasing shot velocity will increases the magnitude of MCRS slightly and increases the CRSL created in target plate. Also, the increase in the shot size results in increased MCRS and CRSL. Also, an increase in the coefficient of friction between the shot surface and the target plate results in an increased magnitude of the maximum residual stress field created in the target plate.

Majzoobi et al. [35], presented simulation of multi – shot impact using a three-dimensional finite element model via LS-DYNA. They concluded that Shot peening process can successfully be simulated by LS-DYNA finite element. Also, increase of velocity improves the residual stress distribution up to a particular point, but further increase in the velocity may reduce the magnitude of MCRS.

Himayat Ullah et al. [36], conducted Explicit dynamics simulation of shot peening process induced by glass and steel shots impact. They investigated that both deformable and rigid shot

models yielded similar results. Also, observed that higher the shot velocity, larger the depth of residual stress and indentation in target plate. Impact with the steel shots caused more indentation and larger volume of plastic deformation than the glass shots due to higher kinetic energy. Furthermore, increasing the shot size resulted in an increase in indentation. However, the surface and subsurface residual stress was negligibly affected by the shot size, velocity, and material.

Gang Wu et al. [37], investigated the effect of shot peening (SP) on residual stress distribution of AISI 304 stainless steel, a 3D dynamic model used for describing single and multiple shot impact phenomenon. Besides, the effects of impact angle, velocity, diameter and coverage on residual stress depth profiles were investigated. The effect of friction on residual stress depth profiles is significant when μ is smaller than 0.2 but can be neglected when the value of μ is larger than 0.2 besides, the shots impact angle must be limited in the range from 60° to 90°for getting a relatively ideal residual stress distribution during SP treatment.

Mekonone, S. T. [5], has been conducted multi-impact shot peening on prealloyed carburized Fe-0.85Mo-0.35C and Fe-1.5Mo-0.3C steels, experimentally. Investigated the effect of shot peening on contact fatigue and wear damage due to surface densification, accumulation of compressive residual stress, and strain hardening. shot peening introduces higher compressive stress at the surface and decreases moving to the depth on a carburized steel.

2.6. Summery

- Shot peening process introduce plastic deformation and residual stress inside the material. Benefit obtained by shot peening are due to the compressive residual stress induced due to local plastic deformation. Shot peening process increases fatigue life, create surface Nano - crystallization and resistance to corrosion fatigue, cracking, and fretting, etc.
- Coverage and intensity are the key parameters which have great influence on the residual stress distribution.
- Maximum compressive residual stress, depth of compressive residual field, and roughness increase while the impact velocity increases.
- The depth of the residual stress maximum in the hard material state increases with rising sphere impact velocity, and in the medium-hard material state it shows a maximum at medium speeds.

- Increase of coverage will increase depth of maximum compressive residual stress and decrease surface compressive residual stress up to certain level, after that the RS vary only negligibly.
- As sphere diameter increases surface and maximum residual stress values slightly changes while the depth of zero crossing and the maximum value of residual stresses are clearly increased, since the kinetic energy of the impacting spheres increases.
- While an increasing yield strength results in rising residual stress surface values and, particularly, in rising maximum values of residual stress, the penetration depths of residual stresses and the depths of the residual stress maxima decrease.
- When workpiece hardness increases, however, penetration depth decreases.
- plastic deformation does not occur for spheres whose hardness is at least double the hardness of the workpiece.
- Incident angle normal or close will produce a good residual stress distribution. since, the peened material get the whole impact energy.
- neither increasing the peening velocity nor coverage can increase the SCRS. To fill this gap, double peening technique provides a potential alternative way. First peening is applied with large size shots, after that the second peening process is applied with smaller shots.

2.7. Gaps identified

As mentioned above, there are numerical studies have been conducted on shot peening process and its impact on the treated material. Nevertheless, they have some limitation such as:

- There are limited number of studies conducted on the effect on carburizing treatment on the residual stress distribution due to shot peening.
- Most of the numerical papers have been used single shot to study shot peening process. however, it is rare to find a single shot peening process in practical application. So single impact does not represent realistic shot peening process.
- Even though they have been used multi-impact the number of shots are very low compared to the actual one.

- They do not take in to account the vertical variation between each consecutive shot. And to obtain stable residual stress distribution the variation should greater than 0.05.
- Apply fixed boundary condition on the lateral side of the target, but infinite boundary condition is recommended.

Chapter Three: Materials and Methods

3.1 Material Data for FEA Model

3.1.1. Material Data of Targets

The materials used throughout this study is pre-alloyed carburized steels. codes, nominal chemical compositions, and type of treatments applied to the materials is shown in table 3.1.

Table 3.1 Code, nominal composition, and applied treatments of the investigated materials.

Material composition	Code	Applied treatments	Power grade
Fe-0.85Mo-0.35C	A85Mo	Carburized	Prealloyed
Fe-1.5Mo-0.3C	AMo1		

Further to the chemical composition of the material, the basic material properties of the targets are presented in below Table 3.2

Table 3.2 Material properties of targets.

Property	Target material	
	Fe-1.5Mo-0.3C	Fe-0.85Mo-0.35C
Density (ton/mm3)	7.4e-9	7.33e-9
Young's modulus (GPa)	208	208
Poisson's ratio	0.28	0.28

Shot-peening process is a nonlinear dynamic contact problem and high strain rate process [25]. Hence must be treated as an impact problem. Some parameters, such as stress wave propagation, strain rate, and strain rate hardening, must be considered in the modeling [38,36,39,9,40] Such behavior of metallic materials is widely elucidated by Johnson-Cook model given as:

$$\sigma = \left[A + B{\varepsilon_{eq}^{p}}^{n}\right]\left[1 + C\ln\frac{\dot{\varepsilon_p}}{\dot{\varepsilon_o}}\right]\left[1 - \left(\frac{T - T_o}{T_{melt} - T_o}\right)^{m}\right]$$

where

$\varepsilon_{eq}^{p}$is equivalent plastic strain, $\dot{\varepsilon}_{p}$and $\dot{\varepsilon}_{o}$ are the applied and reference strain rates,T: applied temperature, T_0: reference temperature and T_{melt}: melting temperature, A is the material yield strength, B and n are work-hardening modulus and exponent, respectively, and C and m are constants describing the flow stress dependency on strain rate and temperature. Shot peening is a cold working process, as previously discussed. Hence, the thermal effect is neglected in this study. The Johnson-cook parameters of the target materials are presented in table below. The hardness (HV) of A85Mo and AMo1 is 649 and 673, respectively [5]. From the hardness we can calculate the yield strength (A) of the steels by using the following equation [68].

$$\sigma_y \text{ (A)} = -90.7 + 2.876(H_V)$$

Johnson-cook parameters are determined by experiment. However, due to the limitation of these data I determined the remaining parameters using curve fitting the residual stresses conducted on the experiment [5]. So as to conduct the finite element simulation of shot peening effectively. But while conducting the fitting I used my best references to make the work more reliable. So, these values listed below table 3.3. When the samples are at room temperature, $\dot{\varepsilon}_{o}$ = 10e-3 [69].

Table 3.3 Johnson-Cook material model parameters of A85Mo and AMo1steels.

	A(MPa)	**B(GPa)**	**n**	**c**	$\dot{\varepsilon}_{o}$
A85Mo	1775.8	50	0.45	0.0001	10e-3
AMo1	1844.5	11	0.51	0.0001	10e-3

3.2.2. Material Data of Shot

The material used for shot is ceramic. The density of the ceramic shot is 3.85×10^3 kg/m3. The Young's modulus and Poisson's ratio of the ceramic shot are 393 GPa and 0.27, respectively. The yield stress of the ceramic shot is about 4000 MPa [41]. Since the yield stress of the ceramic shot material is much higher than that of target carburized steels, the deformation of the shot should be much less than that of the carburized target under the shot peening. moreover, ceramic is brittle and displays little plastic deformation. Therefore, in this study the balls were defined as

rigid bodies since, the hardness of the ceramic shot is higher than that of carburized steels. In addition, rigid shot reduces computational time.

3.2. Numerical Modeling

3.2.1. Model and Analysis Tool (ABAQUS FEA)

ABAQUS FEA is a suite software application for finite element analysis and computer-aided engineering. ABAQUS/CAE or "Complete Abaqus environment", ABAQUS/Standard, ABAQUS/Explicit, Abaqus/CFD or Computational Fluid Dynamics, and Abaqus /Electromagnetic are the five products of ABAQUS FAE [65]. ABAQUS/Explicit, is used to analyze highly dynamic and non-linear problems. Every complete finite element analysis consists of three separate stages [50]:

1. pre-processing, or modeling: in this stage the designer engineer creates an input file for the finite element analyzer.
2. Processing, or finite element analysis: output file is generated from the input file.
3. Post-processing: images, animation, report etc. generated in this stage from the output file. This stage is a visual rendering stage.

3.2.2. Modeling Shot Peening Process

Experimental determination of residual stress has certain limitations, as discussed previously. Differently, FEA simulation can functionally overcome the drawbacks of the experimental means. Finite element method is a promising way for predicting and analyzing all processes. It is used in a number of fields such as solid mechanics, heat transfer and many more. FEM provides an approximate solution of a problem by dividing a structure into a number of small elements, in which the quantity of interest is only allowed to have a simplified spatial variation [42]. In this work, shot peening process is conducted numerically so as to study the distribution of residual stress on the target materials. All SP models in this work has been developed via commercial FEM software ABAQUS/Explicit 2020 and used to investigate multiple shot impacting on the target. Since shot peening is a high-speed process and dynamic effects should be considered, an explicit solver was used for simulations [15]. The principal steps of the simulation are presented in flow chart of Figure. 3.1.

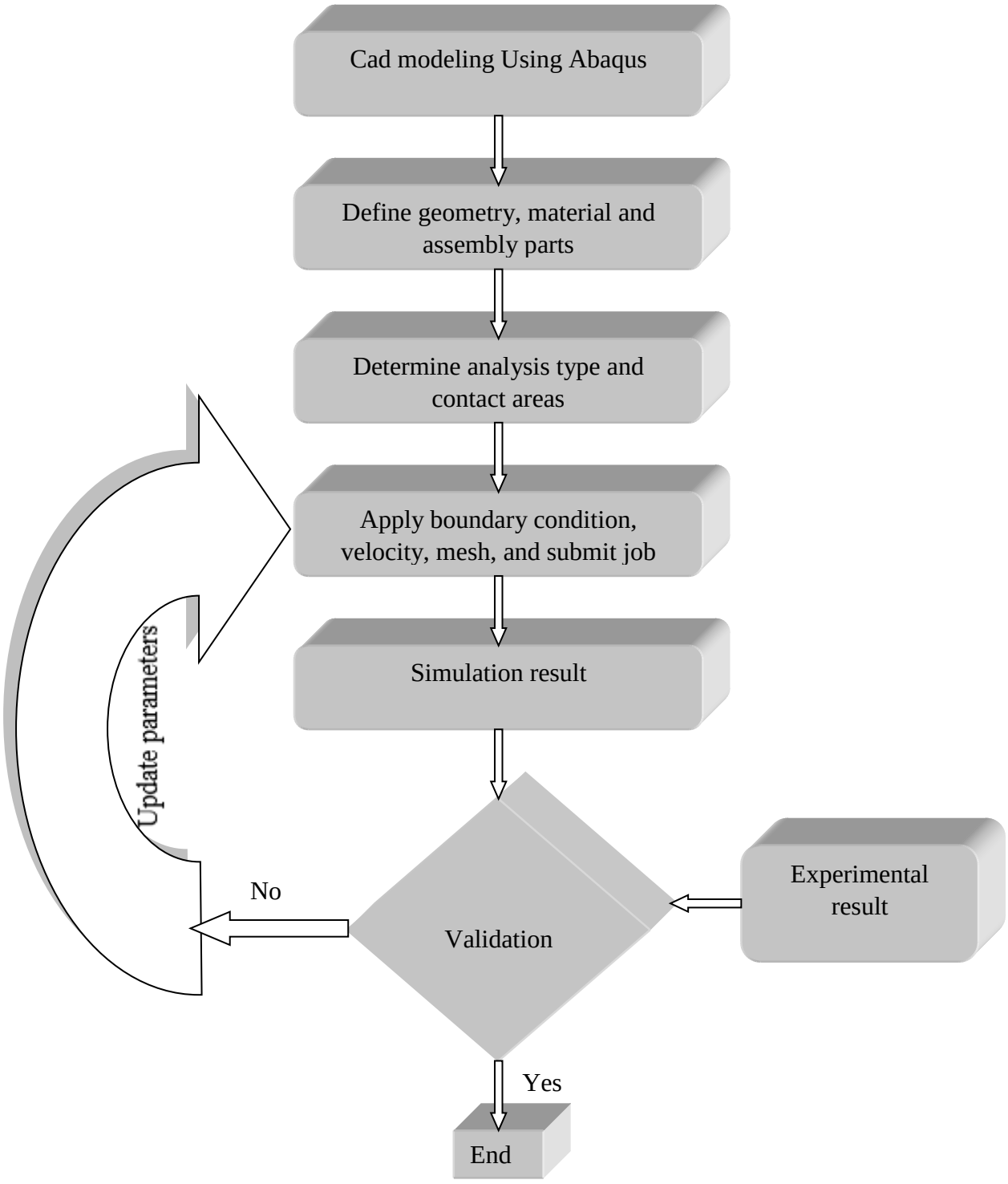

Figure 3.1. Numerical methodology analysis.

General simulation assumptions:

- The target was assumed to be defect-free, isotropic, and elastoplastic materials.
- The velocity of the shot is assumed to be constant and applied to a reference point for each shot as an initial condition to the predefined field.
- A 90° impact angle was used in order to maximize the impact energy transferred to the surface.
- The shot is considered as rigid.

Abaqus has not specific unit for parameters, and the user should select a consistency SI unit system on their own. In this work SI system is chosen as following:

Table 3.4 SI system.

Name	Unit
Length	mm
Force	N
Mass	Tonne
Time	S
Stress	MPa(N/mm^2)
Energy	mJ ($10^{-3}J$)
Density	$tonne/mm^3$

3.3. Simulation Procedure

3.3.1 Modeling Parts

The main model used in this research consisted of two 3-D parts that involved a rectangular-shaped deformable target and a rigid spherical ball. The dimensions of the target plate of 2mm × 2mm × 1mm were kept constant through all the simulations. A circular impact area with a radius of 1mm in the center of the target was considered. The $1mm^2$ impact surface was chosen considering the measured surface of the X-Ray diffractometer to obtain a numerical profile of the residual stresses similar to the experimental profile. The diameter of the shot is 0.35mm made from ceramic.

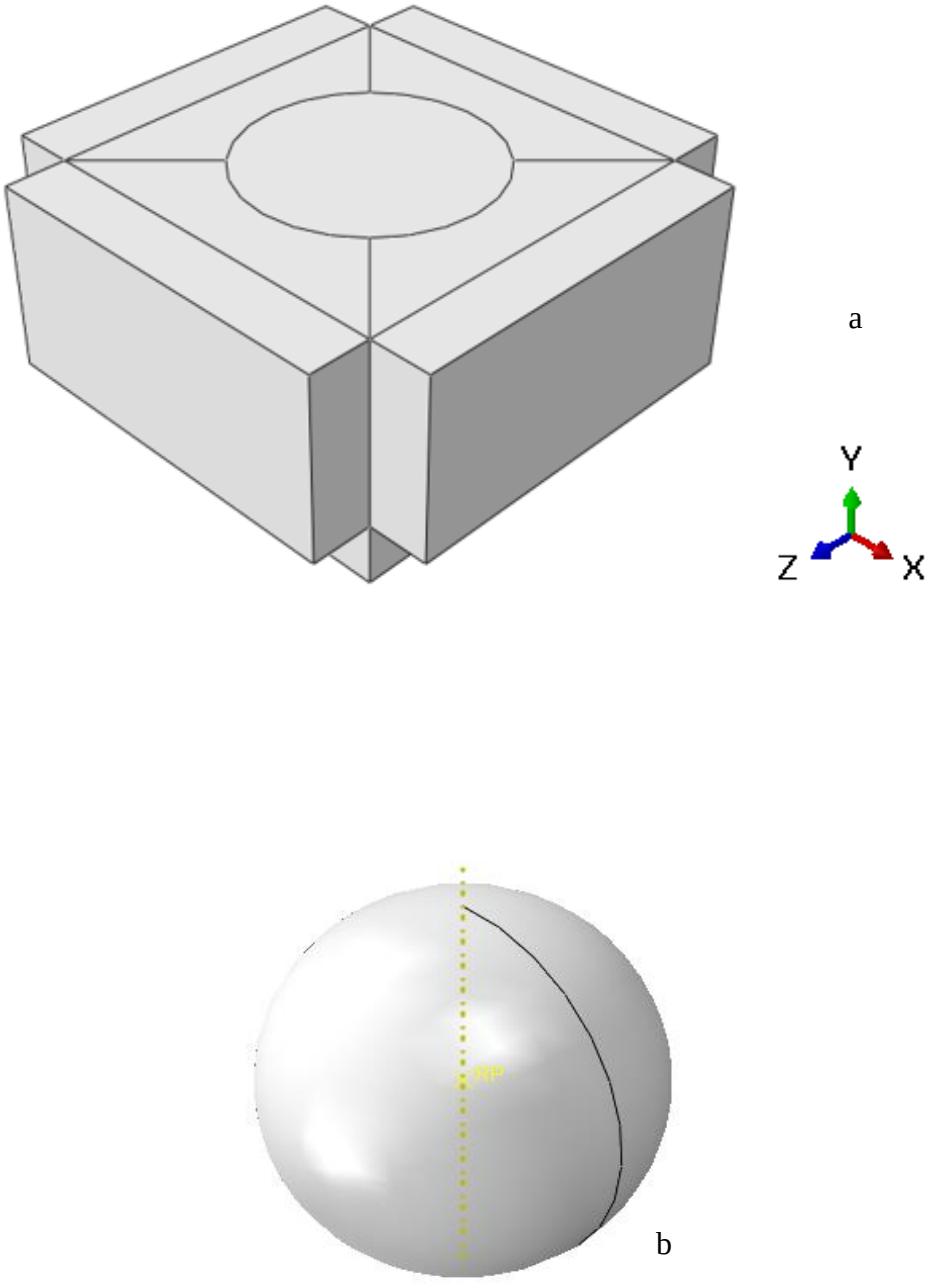

Figure 3.2. Schematic diagram of SP parts: (a) the target; (b) the shot.

3.3.2. Property Module

Material properties, section properties defined here and assign these properties for both the targets and shots. Also, under material properties the elastic and plastic behavior of targets defined. Solid, homogenous section property was assigned for both target and ball. Table 3.2 and 3.3 represents material properties for carburized targets.

Table 3.5 Characteristics of target materials.

Part name	Material behavior	Type	Section type
A85Mo	Elastic-plastic	Isotropic	Solid
AMo1	Elastic-plastic	Isotropic	Solid

3.3.3. Assembly Module

The target and shot created in the part module existed in their own coordinate system, independent of other part. So as to create a single part from instances i.e. target and shot, use the assembly module. Here the parts exist in a global coordinate system, relative to each other. rectangular pattern was used to get the required number of shot so as to get 100% coverage. The total number of shots are 121. If the vertical distance between shot is more than 0.05mm, the residual stress distribution in multi-impact shot tends to stable [44]. The 0.05mm vertical distance between shots ensures that the workpiece material can recover after shot i.e. stress wave of the previous impact disappears before the next shot impact. Based on the above statement, the vertical distance between shots is chosen greater than 0.08mm.

Figure 3.3. Assembly of multiple shot impact parts.

3.3.4. Step Module

Different types of steps create in this module for analyzing the model. In each step, can request different output parameters. Besides, the total time of simulation can be set. As well as the stable time increment in the simulation. In the initial step the system checked everything such as cad model, step time increment, output requested, mesh quality, apply initial residual stress into the target and the velocity at the center of the shot ball. In the first step the shot accelerates in the negative y-direction with a prescribed velocity and impact the target material. The time incrementation scheme in ABAQUS/Explicit is fully automatic and requires no user intervention.

Table 3.6 Step module parameters.

Step	Step Name	Procedure	Time Period	Increment	Nlgeom
0	Initial Step	Initial	N/A	N/A	N/A
1	Step-1	Dynamic, Explicit	0.00018	Automatic	On

3.3.5. Interaction Module

In this module the type of contact between the shots and target defined. The contact relationship between the shot and target is surface to surface, where the ball is the master and the target is the slave. the normal contact behavior between the ball and the target is defined as hard, and the tangential behavior is defined as penalty friction. the depth and distribution of residual stress are in good agreement with the experiment when $0.2 < \mu < 0.6$ [66]. Therefore, choosing $\mu = 0.3$ as friction coefficient in SP model is reasonable.

Table 3.7 Interaction module characteristics.

Interacting parts	Interaction type	Contact property	Normal behavior	Contact formulation	Friction coefficient
Master shots with slave target	General contact (Explicit)	Tangential behavior	Hard contact	Penalty	0.3

3.3.6. Load and Boundary Condition

The load module is used to define boundary condition, predefined fields such as velocity and initial stress. boundary conditions are step dependent i.e. they do not active unless step specifies. some predefined fields are step-dependent, while others are applied only at the beginning of the analysis. Infinite element (AC3D8) with thickness of 0.25mm was used in the lateral and bottom faces of the targets. Also, the degree of freedom of bottom face were restricted. Infinite element used to reduce (elastic shear wave reflection) reflection of dilatational and shear waves back into the region of interest [45,46,47,43]. The ball displacement is fixed in all direction except in the y-direction i.e. $U_1 = U_3 = UR_1 = UR_2 = UR_3 = 0$. It should be noted that typical shot peening velocities range in practice from 20m/s to 120m/s so for the purpose of this model 54m/s is used

to validate with the experiment. Also, the target material had carburized before shot peened and due to carburizing residual stress is developed in the model. And during FEA simulation these residual stresses modeled as initial stress and these stresses presented in table below. To apply these loads, follow this procedure:

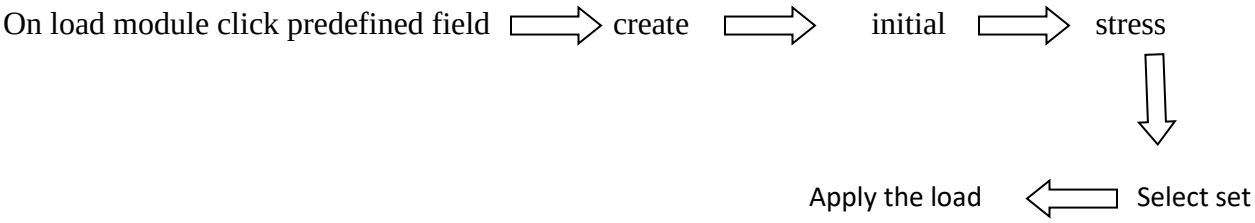

Table 3.8 Residual stresses due to carburizing.

Depth	A85Mo	AMo1
0.001	-25.84	-47.28
0.025	-70	-78
0.05	-116	-110
0.075	-105.5	-99.15
0.1	-95	-95.2
0.125	-84.5	-91.25
0.15	-70	-87.3
0.175	-59.5	-83.35
0.2	-42	-79.4
0.225	-33.5	-54
0.25	-25	-29
0.275	-16.5	-4
0.3	-8	-

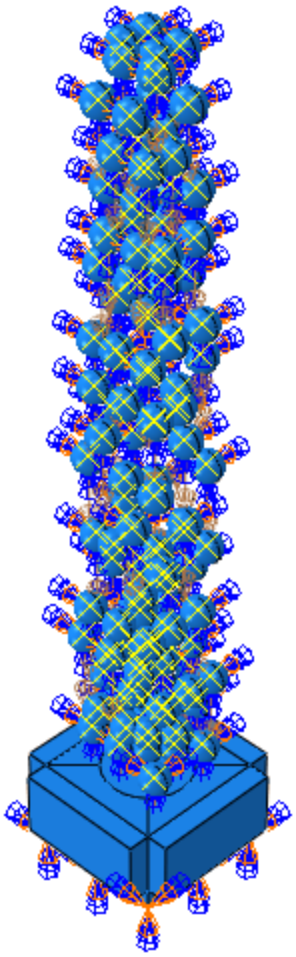

Figure 3.4. 3D model with boundary condition and velocity.

3.3.7. Mesh Module

In this module finite element mesh generated on the parts. Different types of automation and controls are available so that can create a mesh that meets the needs of the analysis. Eight-node linear brick elements with reduced integration and hourglass control (C3D8R) used for the targets. A ten-node modified quadratic tetrahedron (C3D10M) used for the shots. Reduced integration is important to reduce the simulation time in case of high nonlinearities [9]. Besides, these qualities give the capacity of controlling hourglass and eliminating the occurrence of shear locking in problems in which the bending effect is dominant.

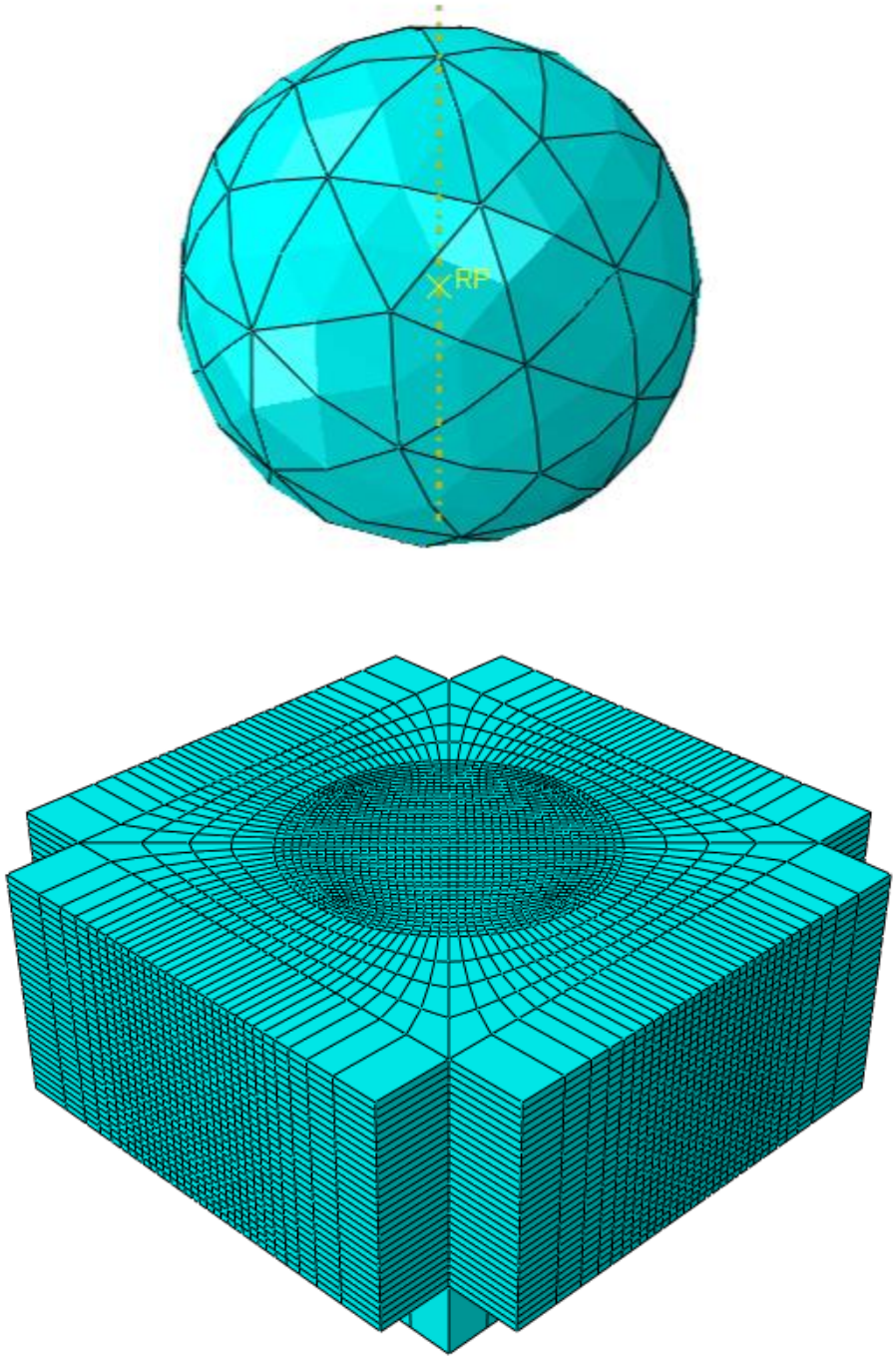

Figure 3.5. The finite element mesh on the instances.

3.3.7.1. Convergence Analysis

Mesh convergence analysis is used to eliminate the dependency of simulation result on the size of the element. simulation accuracy is increased by increasing the density of mesh i.e. smaller element size. However, finer mesh increase degree of freedom of the model, which will increase simulation time and require higher computer capacity. Hence, a compromise between solution accuracy and simulation time is reached by conducting convergence analysis on the model. Four different meshing size from 0.05mm to 0.02mm were used in the analysis. Figure 5.6. illustrates the convergence behavior of the model with mesh size, with respect to the maximum von mises stress in the target. It shows that the von mises stress increases as the mesh size reduced, the von mises stress become nearly constant between mesh size of 0.02 and 0.03mm. Finally, a mesh size 0.025 was chosen in this simulation.

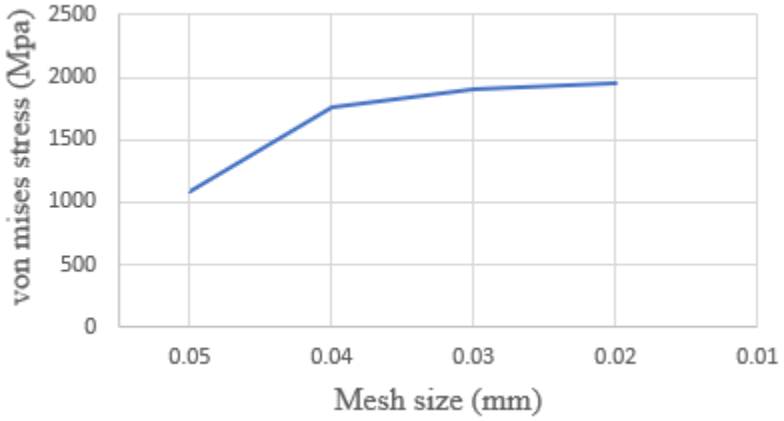

Figure 3.6. Mesh convergence analysis.

Hence, A mesh size of 0.025 * 0.025 * 0.025 mm3 was chose in the impact area. The shot was meshed with element size of 0.09 since it is not our concern. To reduce element distortion under the sever deformations induced by shot impacts, Arbitrary Lagrangian-Eulerian (ALE) meshing technique in Abaqus was applied for the target.

Table 3.9 Mesh characteristics.

Part name	Element size	Element type	Mesh technique
Shot	0.09	C3D10M	Free, tetrahedral
Target	0.025	C3D8R	Sweep, hexahedral

3.3.8. Job Module

ABAQUS/Explicit do not support Acoustic (AC3D8) element, so before submitting the job, first request input file and edit the input file element type i.e. convert AC3D8 to CIN3D8, then import the edited input file as model (figure 3.7. illustrates imported model after converting element type) and create a job on the imported model. Finally submit the job for analysis.

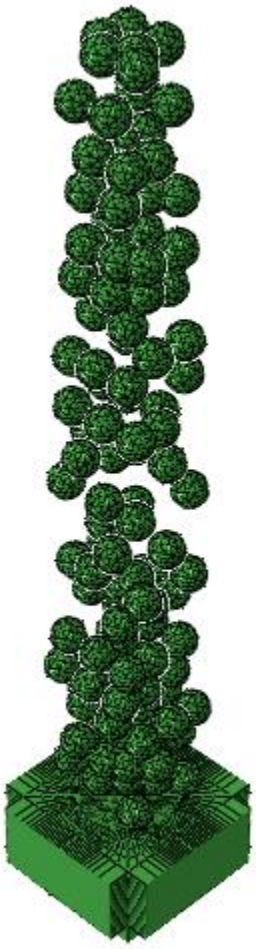

Figure 3.7. Assembly model after converting element type.

3.3.9. Visualization Module

The visualization module is utilized to display the finite element model and result. It gets model and result information from the output database. In the visualization model we can create graph, export simulation results etc.

Chapter Four: Results and Discussion

4.1. Finite Element Method Simulation Result

Results of finite element simulations for the shot-peening-induced impacts using ceramic shot on carburized A85Mo and AMo1 targets are presented in this section. The shot peening impact process is explained in terms of the distribution of residual stress and equivalent plastic strain using shots of 0.35mm diameter at 54 m/s velocity presented. Then the compressive residual stress at interest area (1mm square area) extracted to validate with the experiment result. Finally, the effect of parameters on the resulting residual stress distribution investigated.

Figure 4.1. and figure 4.2. illustrate distribution of residual stress and equivalent plastic strain respectively, after impact for A85Mo target.

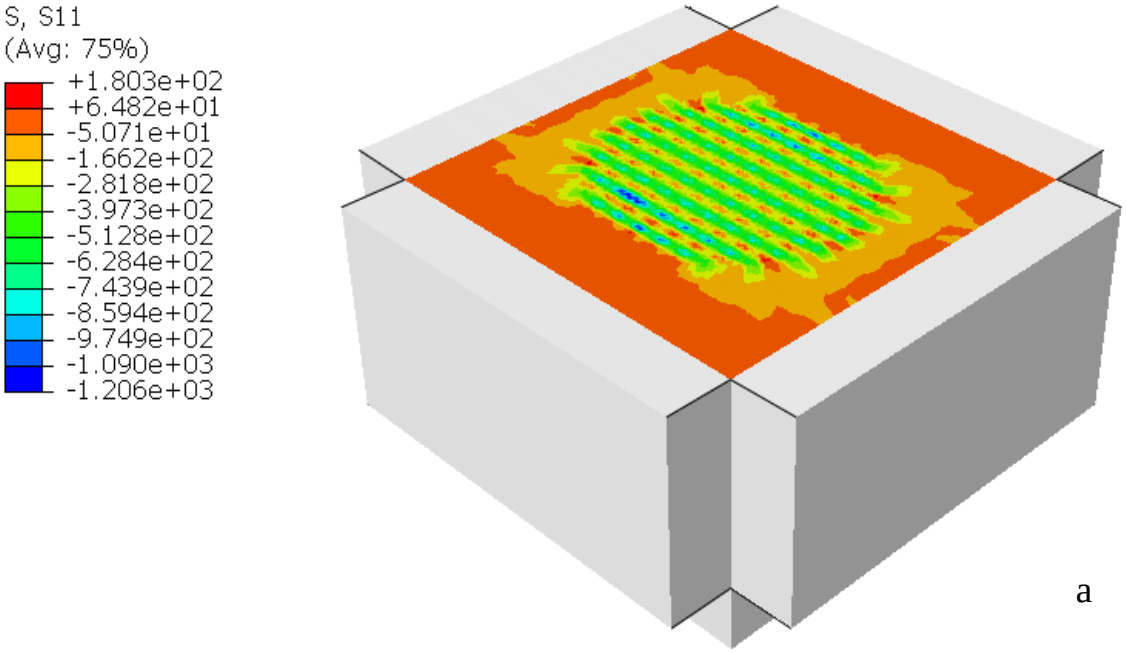

a

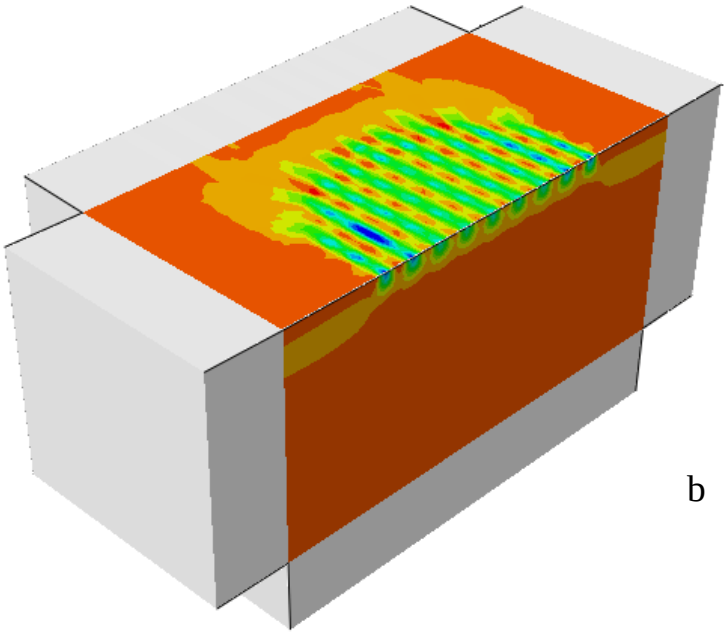

b

Figure 4.1. Distribution of residual stress on the targets after shot peening for A85Mo. a) 3D, b) section view.

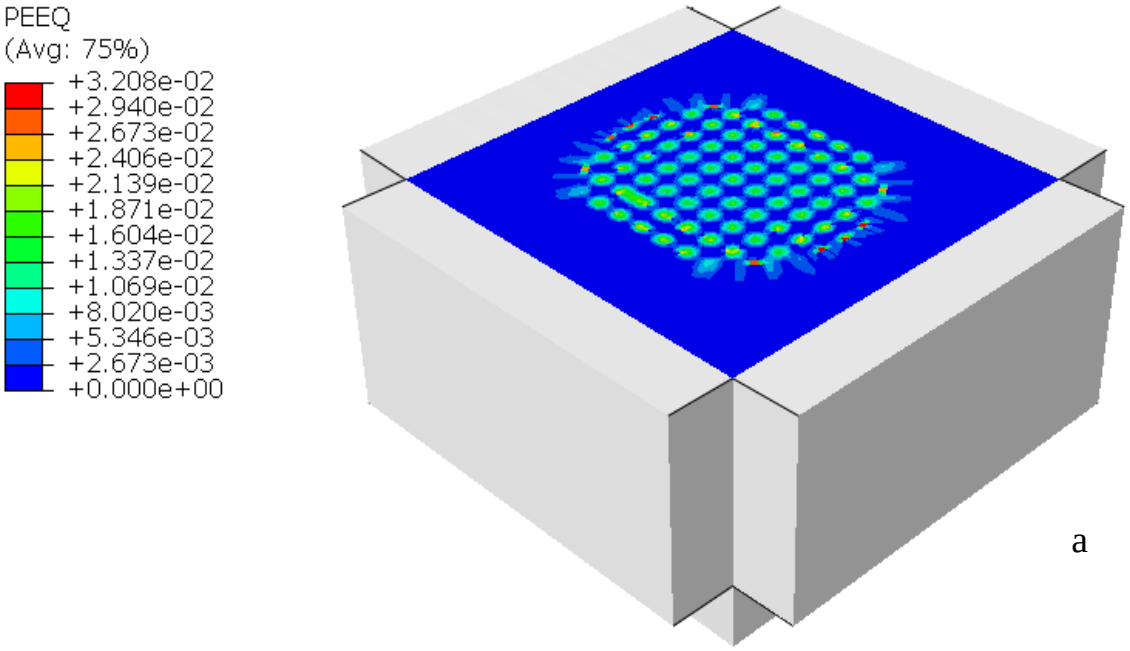

a

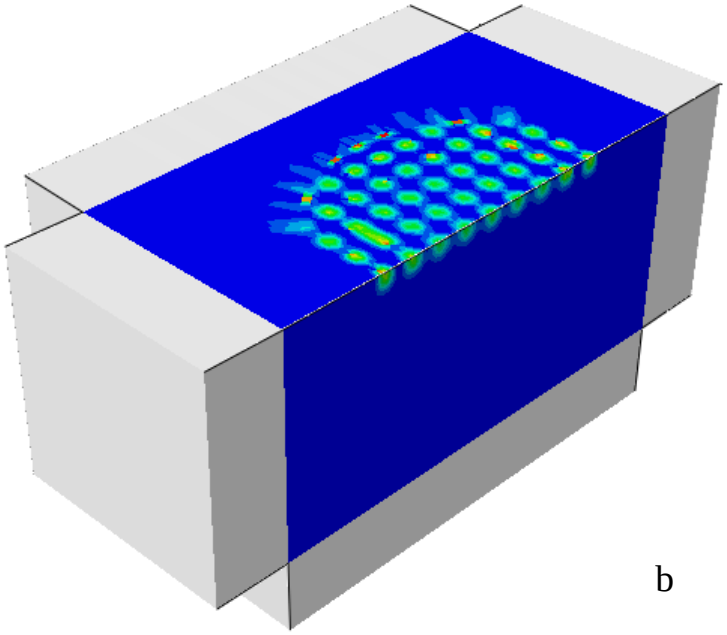

b

Figure 4.2. Distribution of equivalent plastic strain on the targets after shot peening for A85Mo. a) 3D, b) section view.

Similarly, Figure 4.3. and figure 4.4. illustrate distribution of residual stress and equivalent plastic strain for AMo1, respectively.

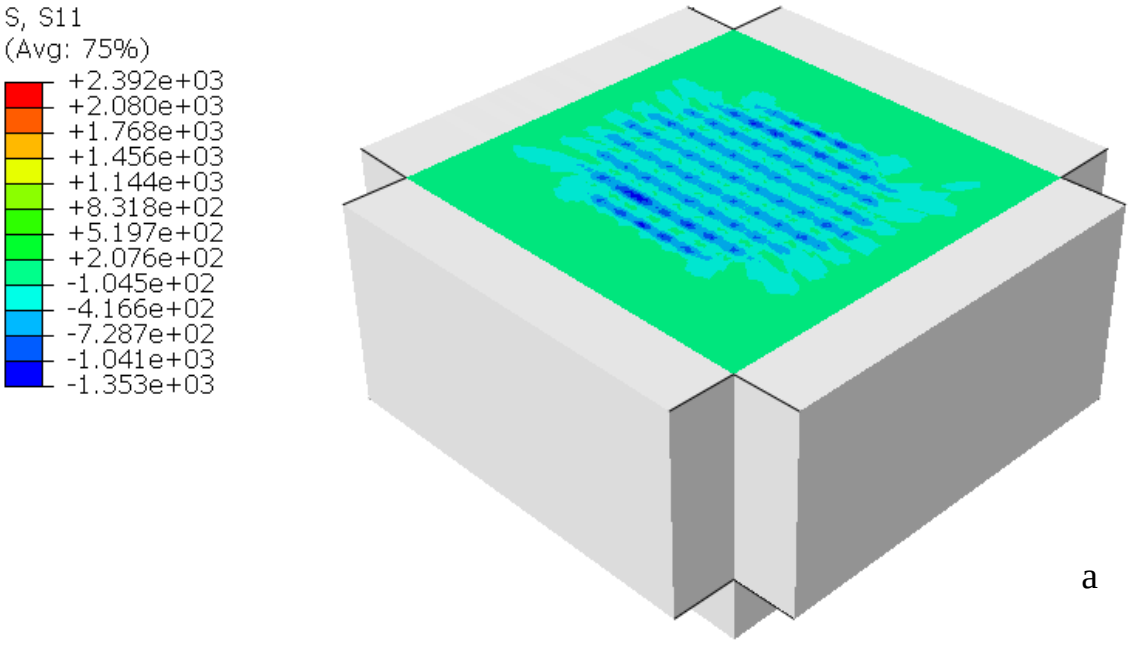

a

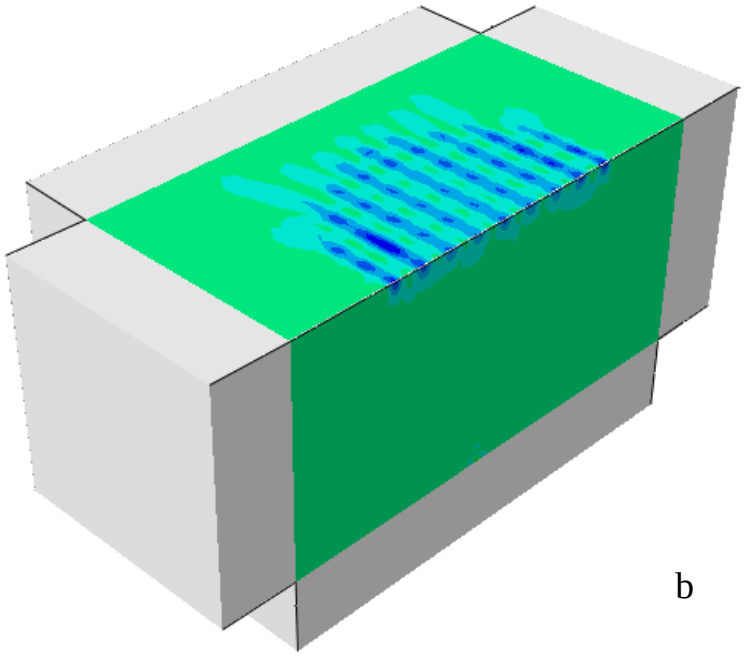

b

Figure 4.3. Distribution of residual stress on the targets after shot peening for AMo1. a) 3D, b) section view.

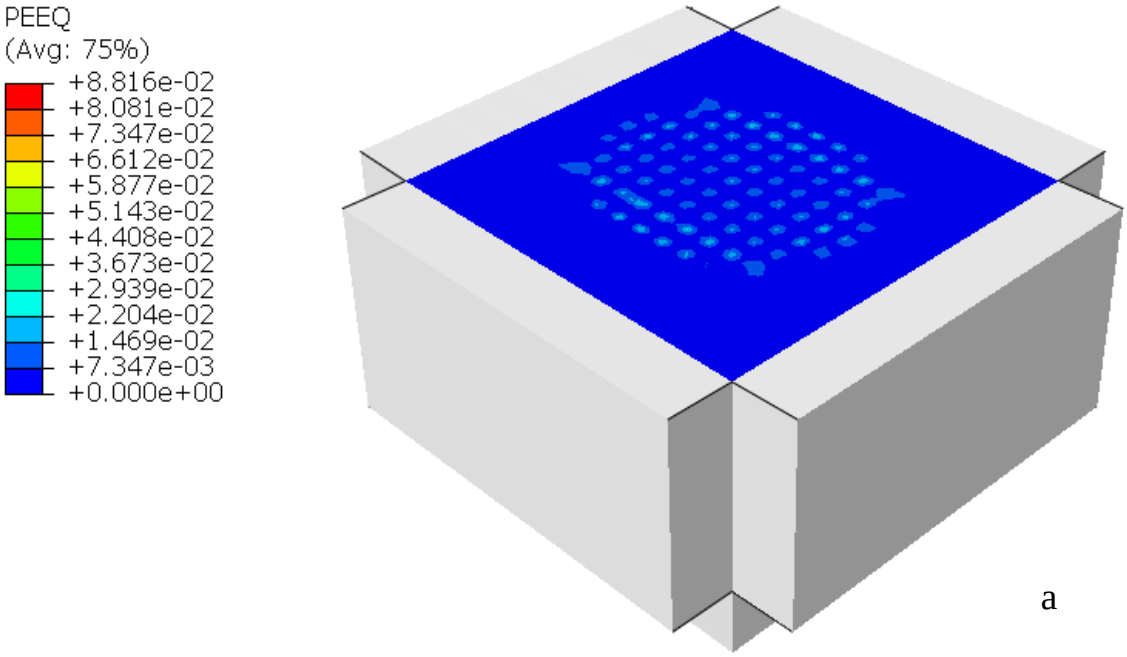

a

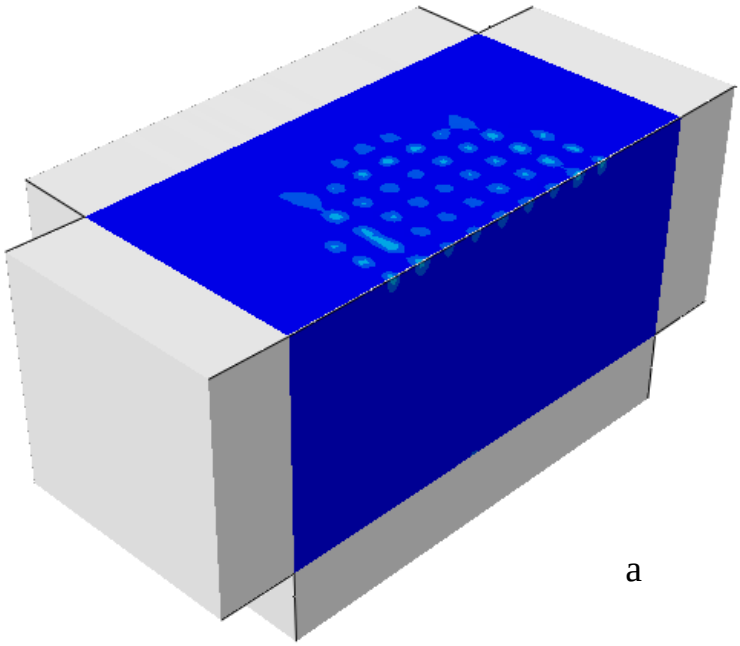

Figure 4.4. Distribution of equivalent plastic strain on the targets after shot peening for AMo1. a) 3D, b) section view.

Due to the impact of many balls compressive residual stress develops on the targets as shown in the above figure 4.1-4.4, and a compressive residual stress layer formed. It can be seen from these figures that the shot peening process mainly induces the residual compressive stress on the targets, and a layer of residual compressive stress may be formed due to the impact of many shots. It is also interesting to notice from the deformed surface that a tensile residual stress is formed due to the propagation of energy from surface to subsurface.

The plastic strain (PE11) in the target materials at point of contact the balls along the center line show in figure 4.5. both the magnitude and depth of plastic strain increased until the shots rebounded. The maximum equivalent plastic strain appeared at the top surface of the target for both A85Mo and AMo1. Then, decreased gradually along the depth direction. And the equivalent plastic strain for A85Mo is greater than AMo1 at the surface, as shown at figure 4.5 c. the is due to the strength of AMo1 is larger than that of A85Mo. this implies as strength of the target material increase, the Permanente deformation at the surface and subsurface will decrease.

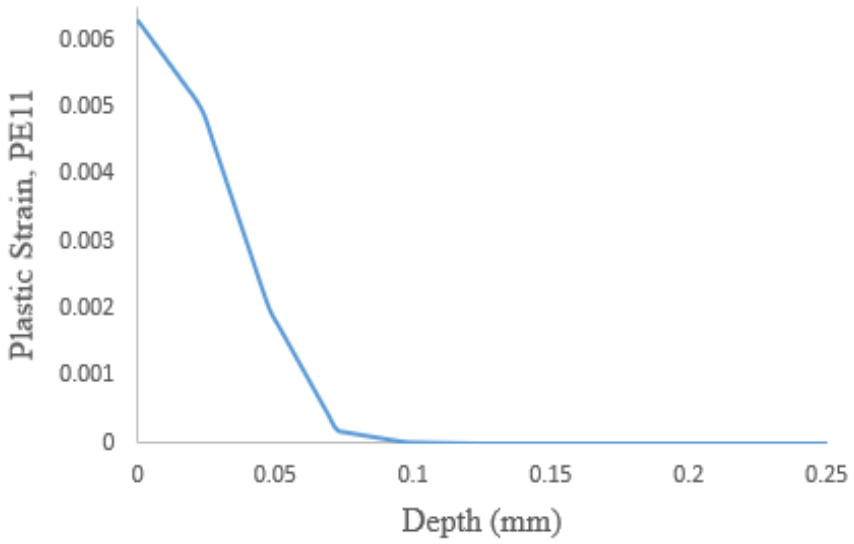
Plastic Strain, PE11
0.006
0.005
0.004
0.003
0.002
0.001
0
0
0.05
0.1
0.15
0.2
0.25
Depth (mm)

a

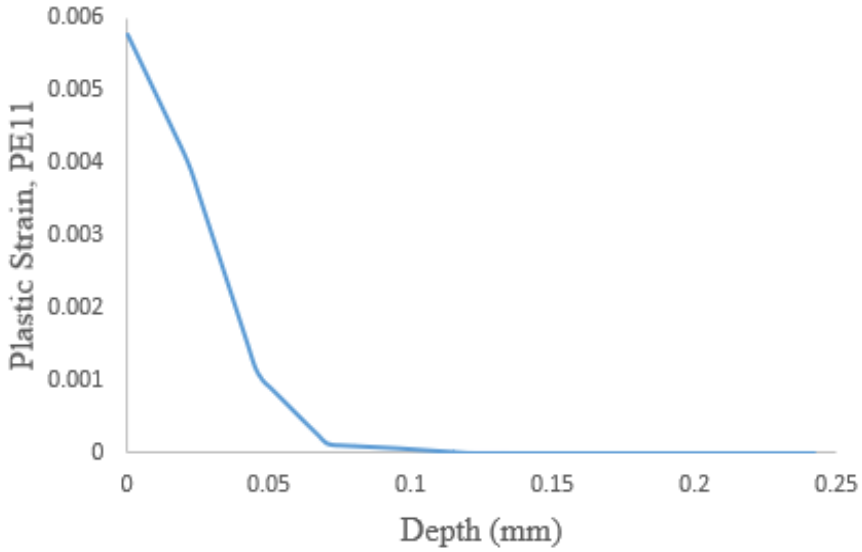
Plastic Strain, PE11
0.006
0.005
0.004
0.003
0.002
0.001
0
0
0.05
0.1
0.15
0.2
0.25
Depth (mm)

b

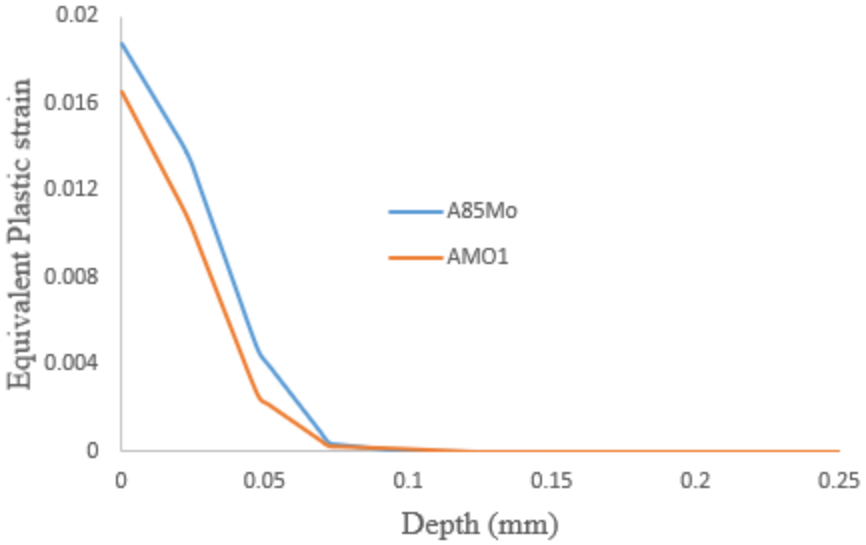

c

Figure 4.5. Distribution of plastic strain along the center line of the target. a) PE,11 for A85Mo, b) PE,11 for AMo1, c) PEEQ for A85Mo and AMo1.

4.2. Comparison Between Measured and Simulated Result

In this section, finite element results are compared with the experimental results from the literature [5]. Multiple-shot model was established to prove the accuracy of numerical model. The averaged residual stresses are compared with the residual stress field from the available experimental results. Figure 4.6. a and b illustrate the simulation and measured results of the residual stress distribution for A85Mo and AMo1 materials, respectively. The error of comparison is around 13% at the surface for A85Mo and 9.04% for AMo1, which support the effectiveness of the simulation model developed in this paper.

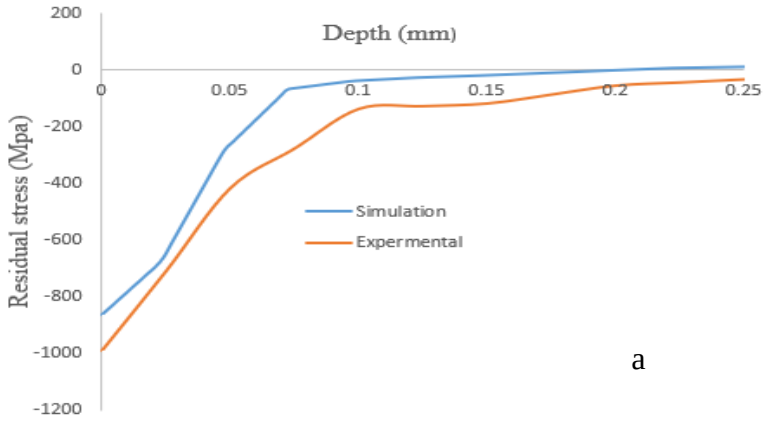

a

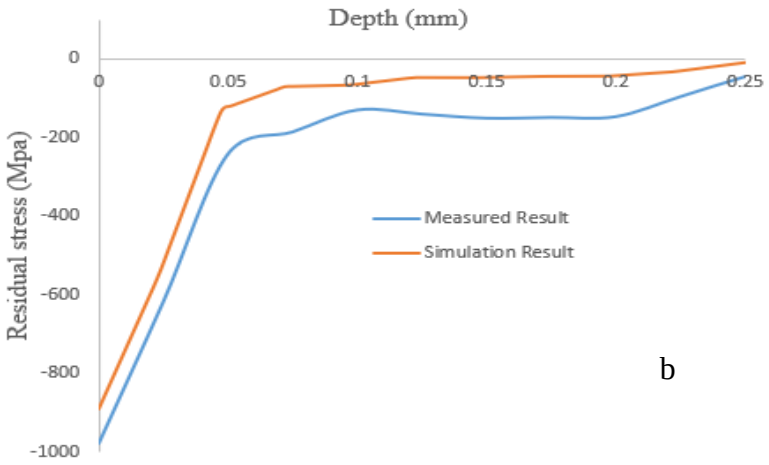

Figure 4.6. Comparison of experimental result with simulation result for: a) A85Mo b) AMo1.

In summary, the comparison of the simulation and experimental results shows good agreement for both A85Mo and AMo1. As presented in the limitation the difference in the results can be due to the variation of material properties along depth and limitation of experimental shot peening date.

[63] studied the distribution of compressive residual stress for several shot peened metals in different states using quantitatively. And developed empirical equation for the surface residual stress. Which is:

$$\sigma_{sur}^{r} = 120 + 0.5(\sigma_y)$$

Now, let's check the validity of the above equation for A85Mo and AMo1.

For A85Mo, the yield strength is 1775.8MPa and substitute this value in the above equation. Get

σ_{sur}^{r}= 1007.9 MPa (compressive)

Similarly, for AMo1 σ_{sur}^{r}= 1042.25 MPa (compressive)

The experimental value For A85Mo and AMo1 is -990.006 MPa and -977.999 MPa, respectively. So, the error between the measured and the calculated value is 1.8 and 6.6%, respectively, which is very low and acceptable.

4.3. Parametric Study

After the validation of the numerical model, the effect of key parameters such as shot velocity, shot size, initial stress, and coverage were investigated. In all of these models the workpiece was carburized A85Mo material for the target and shot used as pervious. Same coverage i.e. 100% used for shot velocity, shot size, and initial stress. The parametric study has been conducted by applying the same shot pattern previously used.

4.3.1. Effect of Shot Velocity

So as to investigate the effect of shot velocity on the residual stress distribution multiple impact shot was used. Four different impact velocity was used: 45, 60, 75 and 90 m/s. as previously stated the shot is rigid with radius 0.35 mm. Figure 4.7. illustrates the variation of residual stress (σ_{xx}) along the center line of depth for the four impact velocities selected. increase in the velocity of shot results in an increase in magnitude of the surface and subsurface residual stress. However, an increase in the velocity of the sot media result in decrease the compressive residual stress layer (CRSL).

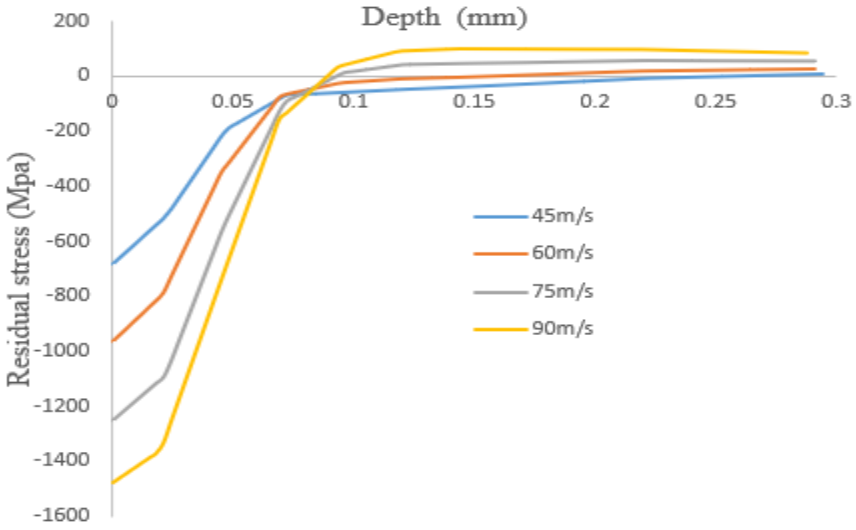

Figure 4.7. Residual stress distribution with different velocities.

4.3.2. Effect of Shot Size

In the similar way, multiple-impact shot finite element analysis was conducted to analyze the effect of shot size by varying the shot sizes. Four shot size were used: 0.2mm, 0.25mm, 0.3mm, and 0.35mm. The velocity of each shot media was assumed constant 60 m/s and friction coefficient μ= 0.3 was considered between each shot surface and target surface. Figure 4.8. shows residual stress (σ_{xx}) variation along the depth for the selected shot sizes. As the shot size increased the magnitude of the surface and subsurface residual stress created in the target increased. However, Compressive residual stress layer decreased as size increased.

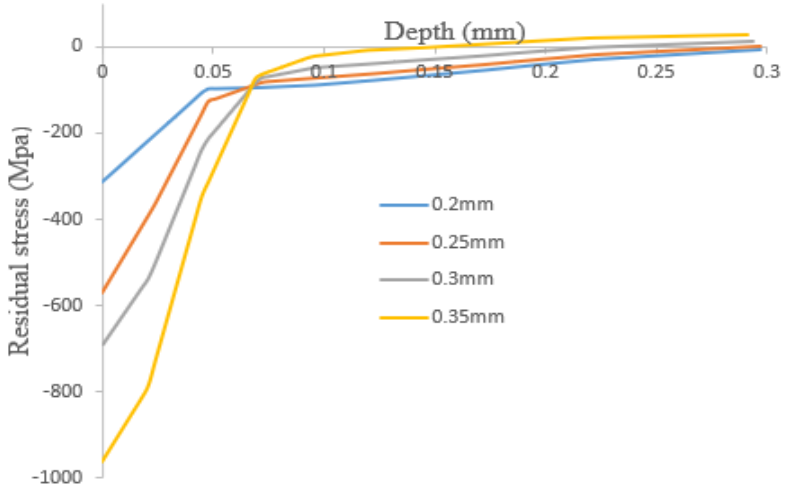

Figure 4.8. Residual stress distribution along centerline with different shot size.

4.3.3. Effect of Initial Residual Stress

The effect of initial residual stress has been conducted here. Assume the velocity and shot size is constant 45m/s and 0.35mm, respectively. As shown in figure 4.9. the surface compressive residual stress is higher for material having initial stress. Also, Initial residual stress results higher compressive residual stress layer. But the depth of CRSL depend on the initial stress depth.

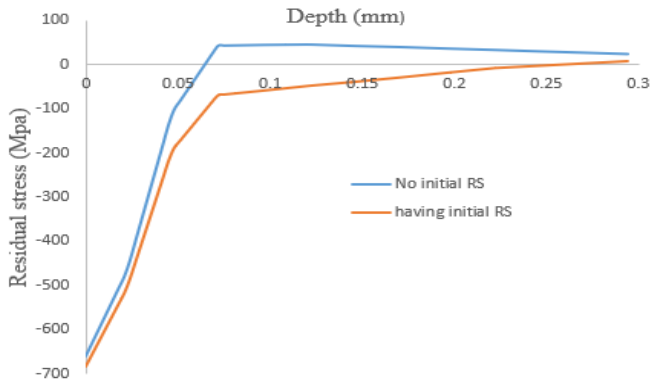

Figure 4.9. Effect of initial stress on residual stress distribution.

4.3.4. Effect of Coverage

As previously stated, coverage is the percentage of peened area during shot peening process. Here, the variation residual stress distribution due to different coverage presented. the velocity and diameter of shot is constant which is 45m/s and 0.35mm, respectively for all coverages. Figure 4.10. illustrate residual stress distribution for various coverages. As coverage increased from 100% to 300%, the surface and subsurface residual stress increased. But depth of compressive residual stress reduced.

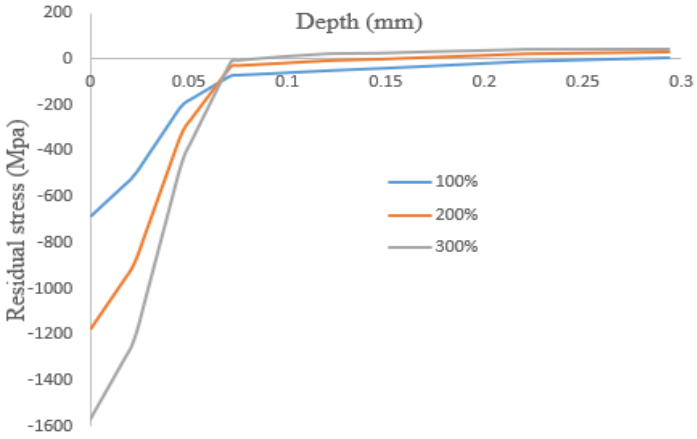

Figure 4.10. Effect of coverage on residual stress distribution.

Chapter Five: Conclusions, Recommendations, and Future Work

5.1. Conclusions

In this paper a ,3D-finite element model consisting of an elasto-plastic carburized Fe-0.85Mo-0.35C and Fe-1.5Mo-0.3C Steel as a target and a rigid ceramic shots bead were developed. In the simulation, the program of ABAQUS /Explicit was used for the 3D finite element dynamic analysis. The simulation results were validated by comparison of the residual stress profiles obtained by simulation and the X-Ray diffraction experiment results. The effect of shot velocity, shot size, initial stress, and coverage upon the variation of residual stress have been investigated and discussed. Based on the results, following points can be concluded.

- The process of shot peening can be successfully simulated with the help of commercial finite element code ABAQUS/Explicit. This finite element analysis is useful for the investigation of the influence of various parameters on the shot peening process with low cost and time.
- Increasing shot velocity, shot diameter result in an increase in surface residual stress. However, the depth of compressive residual stress reduced significantly.
- Initial stress in a peened material result in an increase surface compressive residual stress and depth of compressive residual stress layer.
- A good agreement has been found between the simulated and measured result for carburized Fe-0.85Mo-0.35C and Fe-1.5Mo-0.3C Steel materials.
- Shot peening improves the material resistance to fatigue, stress corrosion, and crack development and crack propagation. Also, it used to create nanocrystalline surface.

5.2. Recommendations

Shot peening is a very complex process involving dynamic analysis of fast-moving shot impacting on a metallic target. There are a significant number of parameters involved in shot peening which need to be controlled and regulated in order to produce a more beneficial compressive residual stress distribution within the target. Unless uncontrolled shot peening process results crack and high roughness on the peened surface material. Besides, on the study results the following points are important for future work:

- Use explicit solver greatly help to handle the dynamic system of the shot peening process.
- Using infinite element in the lateral and bottom faces as a boundary condition makes the analysis realistic and prevent elastic shear wave reflection.
- Use Johnson cook material plasticity model to describe the material elastic-plastic properties.
- Provide enough distance between successive shots makes the residual stress distribution in multi-impact shot more stable.
- During coverage greater than 100% use the first simulation result as input for the second simulation and so on.
- Use high process computers reduce total time of analysis and able to apply fine mesh in the mesh module.

5.3. Future Work

In this thesis, the residual stress pattern due to multiple impact on a carburized steel, was modelled using finite element analysis. As discussed earlier, a simplified assumption was used regarding the material behavior. However due to carburization the material properties vary along the thickness direction. Thus, further study needed by considering the variation of material properties through the thickness so as to obtain accurate result.

Reference

[1] Hong, T., Ooi, J.Y., Favier, J., and Shaw, B. (2008). A numerical simulation to relate the shot peening process parameters to the induced residual stresses, Engineering Failure Analysis. 15(8) 1097-1110, doi:10.1016/J.ENGFAILANAL.2007.11.017.

[2] Jebahi, M., Gakwaya, A., Lévesque, J., Mechri, O., and Ba, K. (2016). Robust methodology to simulate real shot peening process using discrete-continuum coupling method. International Journal of Mechanical Sciences, Elsevier, 107, 21-33. 10.1016/j.ijmecsci.2016.01.005. hal-02378529.

[3] https://www.substech.com/dokuwiki/doku.php?id=shot_peening.

[4] Murugaratnam, K., Utili, S., Petrinic, N. (2015). A combined DEM-FEM numerical method for shot peening parameter optimization. Advanced in engineering software, 79, 13-26. doi: 10.1016/j.advengsoft.2014.09.001.

[5] Mekonone, S. T. (2018). Theoretical analysis and experimental investigation of contact fatigue and surface damage in prealloyed and diffusion bonded sintered steels. PhD thesis, University of Trento, Italy. http://eprints-phd.biblio.unitn.it/3032/.

[6] Bhuvaraghana, B., Srinivasan, S. M., Maffeo, B., McCLain, R. D., Potdar, Y., & Prakash, O. (2010). Shot peening simulation using discrete and finite element methods. Advances in Engineering Software, 41(12), 1266–1276. doi: 10.1016/j.advengsoft.2010.09.003.

[7] Maleki.E, Unal.O (2020). Optimization of Shot Peening Effective Parameters on Surface Hardness Improvement. Metals and Materials International. doi:10.1007/s12540-020-00758-x.

[8] S. Shen, Z. D. Han, C. A. Herrera, S. N. Atluri (2004). Assessment, Development, and Validation of Computational Fracture Mechanics Methodologies and Tools for Shot-Peened Materials Used in Rotorcraft Principal Structural Elements. FAA report DOT/FAA/AR-03/76.

[9] Ullah.H, Ullah.B, Rauf.A, and Muhammad.R (2018). Dynamic finite element analysis of shot peening process of 2618-T61 aluminum alloy. Scientia Iranica, 26, 1378–1387. doi.10.24200/sci.2018.5483.1302.

[10] Trung, P. Q. (2017). Experimental and numerical investigation on shot peening of low alloy steel. PhD thesis, Nanyang Technological University.

[11] Savas, S. (2010). Monitoring Variation of Surface Residual Stresses in the Shot Peened Steel Components by Magnetic Barkhausen Noise Method. MSc thesis, Middle East Technical University.

[12] Ahmad, A. S., Wu, Y., & Gong, H. (2020). Coupled finite and discrete element shot peening simulation based on Johnson–Cook material model. Proceedings of the Institution of Mechanical Engineers, Design and Applications, 234(7), 974–987. doi:10.1177/1464420720921211.

[13] Hong, T., Ooi, J.Y., Favier, J., and Shaw, B. (2008). A numerical study of the residual stress pattern from single shot impacting on a metallic component. Advanced in Engineering Software, 39(9), 743-756. doi: 10.1016/j.advengsoft.2007.10.002.

[14] Xie, L., Wang, C., Wang, L., Wang, Z., Jiang, C., Lu, W., & Ji, V. (2016). Numerical analysis and experimental validation on residual stress distribution of titanium matrix composite after shot peening treatment. Mechanics of Materials, 99, 2 8. doi: 10.1016/j.mechmat.2016.05.005

[15] Chadwick, D. j. (2016). Mechanism of shot peening enhancement for the fatigue performance of AA7050-T7451. MSc thesis, Purdue University. https://docs.lib.purdue.edu/open_access_theses/839.

[16] Franchim, A. S., Campos, V. S. de, Travessa, D. N., & Neto, C. de M. (2009). Analytical modelling for residual stresses produced by shot peening. Materials and Design, 30(5), 1556–1560. doi: 10.1016/j.matdes.2008.07.040.

[17] https://www.airblast-abrasives.com/products/non-metallic-abrasives/ceramic-beads.

[18] https://www.finishingsystems.com/abrasives/steel-shot/.

[19 https://saic-uk.co.uk/product/glass-bead-shot-blasting-abrasive-25kg-1-tonne/.

[20] Rahimzadeh, T. (2009). finite element modelling of residual stresses due to shot peening. MSc thesis, McGill University.

[21] https://www.weerg.com/en/global/blog/the-advantages-of-shot-peening.

[22] Mitra, S. (2016). Finite element surface analysis of cosmetic finishing applications – Shot Peening. MSc thesis. doi: 10.13140/RG.2.2.23540.55688

[23] Świetlicki, A., Szala, M., and Walczak, M. (2022). Effects of Shot Peening and Cavitation Peening on Properties of Surface Layer of Metallic Materials-A Short Review. Materials (Basel), 15(7), 2476. doi: 10.3390/ma15072476.

[24] Romero, J.S. (2002). Optimization of the shot peening process in terms of fatigue resistance. PhD thesis, University of Sheffield, U.K.

[25] Cheng, X. (2007). Experimental and numerical approaches for improving rolling contact fatigue of bearing steel through enhanced compressive residual stress. PhD thesis, Ohio State University.

[27] Herzog., Zinn, B., Scholtes, B., and Wohlfarth, H. (1996). The significance of Almen Intensity for the Generation of Shot Peening Residual Stresses. University of Gh Kassel, Germany.

[28] OGAWA, K., & ASANO, T. (2000). Theoretical Prediction of Residual Stress Produced by Shot Peening and Experimental Verification for Carburized Steel. Journal of the Society of Materials Science, Japan, 49(3), 55–62. doi: 10.2472/jsms.49.3appendix_55.

[29] MATARNEH, M.E. (2016). Modeling of fatigue life by shot peening. International Journal of Mechanical Engineering (IJME), 5(6). ISSN(P): 2319-2240; ISSN(E): 2319-2259.

[30] Sherafatnia, K., Farrahi, G. H., & Mahmoudi, A. H. (2018). Effect of initial surface treatment on shot peening residual stress field: Analytical approach with experimental verification. International Journal of Mechanical Sciences, 137, 171–181. doi: 10.1016/j.ijmecsci.2018.01.022.

[31] Mylonas, G. I., & Labeas, G. (2011). Numerical modelling of shot peening process and corresponding products: Residual stress, surface roughness and cold work prediction. Surface and Coatings Technology, 205(19), 4480–4494. doi: 10.1016/j.surfcoat.2011.03.080.

[32] Lin, Q., Liu, H., Zhu, C., Chen, D., & Zhou, S. (2020). Effects of different shot peening parameters on residual stress, surface roughness and cell size. Surface and Coatings Technology, 398, 126054. doi: 10.1016/j.surfcoat.2020.126054.

[33] Meguid, S. A., Shagal, G., & Stranart, J. C. (2002). 3D FE analysis of peening of strain-rate sensitive materials using multiple impingement model. International Journal of Impact Engineering, 27(2), 119–134. doi:10.1016/s0734-743x (01)00043-4.

[34] Manoucherifar, A., and Rezvani, K. (2011). 3D FE analysis of shot peening process for simulation and research on shot peening process parameters. Conference paper.

[35] Majzoobi, G. H., Azizi, R., and Alavi Nia, A. (2005). A three-dimensional simulation of shot peening process using multiple shot impacts. Journal of Materials Processing Technology, 164-165, 1226–1234. doi: 10.1016/j.jmatprotec.2005.02.139.

[36] Ullah, H., Rauf, A., Ullah, B., Rehan, M., and Muhammad, R. (2018). Explicit dynamics simulation of shot peening process induced by various types of shots impacts. Journal of the Brazilian Society of Mechanical Sciences and Engineering, 40(2). doi:10.1007/s40430-018-1031-x.

[37] Wu, G., Wang, Z., Gan, J., Yang, Y., Meng, Q., Wei, S., & Huang, H. (2018). FE analysis of shot-peening-induced residual stresses of AISI 304 stainless steel by considering mesh density and friction coefficient. Surface Engineering, 1 13. doi:10.1080/02670844.2018.1470817.

[38] WANG, J., and LIU, F. (2011). Numerical simulation for shot-peening based on sph-coupled fem. International Journal of Computational Methods, 08(04),731 -745. doi:10.1142/s0219876211002782.

[39] Donzella, G., Pola, A., Solazzi, L., and Marconi, G. P. (2000). Effect of shot peening on carburized surfaces. International Journal of Materials and Product Technology, 15(1/2), 117. doi:10.1504/ijmpt.2000.001240.

[40] Zhang, Y., Lai, F., Qu, S., Ji, V., Liu, H., and Li, X. (2020). Effect of shot peening on residual stress distribution and tribological behaviors of 17Cr2Ni2MoVNb steel. Surface and Coatings Technology. doi: 10.1016/j.surfcoat.2020.125497.

[41] Cheng, Y. (2020). Experimental and Numerical Investigation of Residual Stresses in Shot Peened Flange Pin of Landing Gears. MSc thesis, Carleton University, Ottawa, Ontario.

[42] Persson, P. (2016). Finite element analysis of hot rolling in the blooming mill. MSc thesis.

[43] Zhao, J., Tang, J., Ding, H., Shao, W., Zhao, X., Liu, H., & Jiang, T. (2021). A numerical and experimental investigation on the evolution of three-dimensional surface topography of 12Cr2Ni4A steel in shot peening. Journal of Manufacturing Processes, 70, 259–270. doi: 10.1016/j.jmapro.2021.08.032.

[44] Wang, Z., Shi, M., Gan, J., Wang, X., Yang, Y., & Ren, X. (2021). The Effects of Shot Distance and Impact Sequence on the Residual Stress Field in Shot Peening Finite Element Model. Metals, 11(3), 462. doi:10.3390/met11030462.

[45] Schwarzer, J., Schulze, V., & Vöhringer, O. (2006). Finite Element Simulation of Shot Peening - A Method to Evaluate the Influence of Peening Parameters on Surface Characteristics. Shot Peening, 505–515. doi:10.1002/3527606580.ch65.

[46] HU, D., GAO, Y., MENG, F., SONG, J., WANG, Y., REN, M., and WANG, R. (2017). A unifying approach in simulating the shot peening process using a 3D random representative volume finite element model. Chinese Journal of Aeronautics, 30(4), 1592–1602. doi: 10.1016/j.cja.2016.11.005.

[47] Astaraee, A. H., Bagherifard, S., Bradanini, A., Duó, P., Henze, S., Taylor, B., and Guagliano, M. (2020). Application of shot peening to case-hardened steel gears: The effect of gradient material properties and component geometry. Surface and Coatings Technology, 126084. doi: 10.1016/j.surfcoat.2020.126084.

[48] Barrios, D.B., Angelo, E., Gonçalves, E. (2005). Finite element shot peening simulation for residual stress. Analysis and comparison with experimental results.

[49] Murugaratnam, K. (2016). A refined numerical modelling technique for Shot Peening. PhD thesis, University of Oxford.

[50] Yuting, Q., and Junyi, X. (2012). Abaqus simulation of residual stress induced by waterjet peening. MSc thesis, Blekinge Institute of Technology, Karlskrona, Sweden.

[51] Hassanzadeh, M., Moussavi Torshizi, S. (2022). Multi-objective Optimization of Shot-peening Parameters using Design of Experiments and Finite Element Simulation: A Statistical Model. Journal of Applied and Computational Mechanics, 8(3), 838-852. doi: 10.22055/jacm.2020.33102.2152.

[52] Peng, R.L., Elfsberg, J., and Ahmad, M. (2016). Increased fatigue strength of cast iron components through optimization of residual stresses-Part II. Project within FFI Vehicle Development program.

[53] Wu, D., Yao, C., & Zhang, D. (2017). Surface characterization of Ti1023 alloy shot peened by cast steel and ceramic shot. Advances in Mechanical Engineering, 9(10), doi:10.1177/1687814017723287.

[54] Wei, Q., Wu, W., He, W., Zhu, J., & Zhang, J. (2018). 3D Finite Element Simulation of Shot Peening Using A Sequential Model with Multiple-Shot Impacts. International Journal of Computational Methods, doi:10.1142/s0219876218501372.

[55] Dinesh Mahajan, D., Sadaphal, D.B., and Swapnil Kulkarni, S. (2014). Evaluating the Effect of Shot Peening as A Surface Treatment Process for Inducing residual compressive stresses using FEA. International Journal of Advanced Engineering Research and Studies.

[56] Gebretsadkan, A. Numerical modeling mixed mode surface fracture of carburized Fe-0.85Mo-0.3C steel subjected to rolling-sliding contact. MSc thesis, Addis Ababa university, Ethiopia.

[57] Metinöz, I. (2014). Dry sliding and contact fatigue behavior of different high-density Ni-Cu-Mo PM Steels. PhD thesis, University of Trento-Italy.

[58] Walvekar, A. A., & Sadeghi, F. (2017). Rolling contact fatigue of case carburized steels. International Journal of Fatigue, 95, 264–281. doi: 10.1016/j.ijfatigue.2016.11.003.

[59] Emanuelli, L., Biesuz, M., Libardi, S., Marconi, P., and Malinari, A. (2015). Shot peening of a sintered Ni-Cu-Mo steel produced by diffusion bonded powders. La Metallurgia Italiana, 107(3), 23-28.

[60] Chaieb, I., Ben Moussa, N., Ben Fredj, N., & Ben Salah, N. (2021). An innovative contactless finite element simulation of the shot peening process. The International Journal of Advanced Manufacturing Technology, 113(7-8). doi:10.1007/s00170-021-06809-w.

[61] Abadie, F.X., Beaudonnet, A.L., Dixon, J., Fader, J., Fabre, A., and Barrallier, L. (2008). Application of ceramic shot for peening of automotive suspension coil springs. ICSP-10, Tokyo, Japan.

[62] WANG, C., HU, J., GU, Z., XU, Y., and WANG, X. (2017). Simulation on Residual Stress of Shot Peening Based on a Symmetrical Cell Model. Chinese Journal of Mechanical Engineering, 30(2), 344–351. doi:10.1007/s10033-017-0084-6.

[63] Wang, S., Li, Y., Yao, M., & Wang, R. (1998). Compressive residual stress introduced by shot peening. Journal of Materials Processing Technology, 73(1-3), 64–73. doi:10.1016/s0924-0136(97)00213-6.

[64] Singh, G. (2009). Effective Simulation and Optimization of a Laser P e Simulation and Optimization of a Laser Peening Process. PhD thesis, Wright State University.

[65] https://en.wikipedia.org/wiki/Abaqus.

[66] FE analysis of shot-peening-induced residual stresses of AISI 304 stainless steel by considering mesh density and friction coefficient.

[67] Long, J. M., Wang, G. F., Feng, X. Q., and Yu, S. W. (2014). Influence of surface tension on fractal contact model. Journal of Applied Physics, 115(12), 123522. doi:10.1063/1.4869742.

[68] Yang J.J., Pang K.J. Elastoplastic behavior of case-carburized 18Cr2Ni4WA steel by indenter testing. *J. Aerosp. Eng*. 2019;32: 04019045.doi: 10.1061/(ASCE)AS.1943-5525.0001035.

[69] Pang, L, Liu, G C, & Lu, J P (Dec 2015). The experiments for mechanical properties of 20Cr2Ni4 steel and the coefficient definition of constitutive equation. IOP Conference Series Materials Science and Engineering (Online), 103(1), 7. doi:101088/1757-899X/103/1/012028